Simulation of Solid State MAS NMR Spectra: Spin Half Nucleus Coupled to Quadrupolar Nucleus

by

Hermann Kampermann

Submitted to the Department of Chemistry in accordance with the requirements of Chemistry 4GO6

April 2000

McMaster University

Hamilton, Ontario, Canada

Abstract

This project comprises the testing and development of a new simulation program for MAS NMR spectra of solid samples. The specific goal is the treatment of the effect on the spectrum of a spin-$\frac{1}{2}$ nucleus due to a dipolar coupled quadrupolar nucleus. The simulation program is based on an average Hamiltonian approach, which eliminates the large Zeeman and quadrupolar interactions from the Hamiltonian. The averaged Hamiltonian is then used in Floquet theory to calculate the spectrum. The new approach is tested by comparison with perturbation approaches and experimental data. Different systems are considered, with principle attention given to ^{13}C labeled acetanilide, which exhibits residual dipolar coupling to the ^{14}N-spin. The syntheses, X-ray single-crystal structure determination and CP/MAS NMR data, at different B_0-fields, are also presented.

Acknowledgements

I wish to express my gratitude to my supervisors Dr. R. S. Dumont and Dr. A. D. Bain for their immense guidance and support throughout this work. I wish to thank Dr. H. Grondey (Toronto) for their immense help with the solid state NMR spectrometers and Dr. P. H. M. Harrison for his assistance during my experimental work in his lab.

I would like to thank the Chemistry Department for giving me the opportunity to study at McMaster. I am also grateful to the DAAD for their financial support.

I am grateful to the many people who have offered their friendship and support throughout my stay at McMaster. In particular I would like to thank Paul Hazendonk for his assistance in solving theoretical problems and his help with the NMR spectrometers.

My thanks, also, to Karsten Koppe, my parents and my brother for their help and support throughout this year.

I especially thank my girlfriend, Bärbel, for her love and encouragement during my stay in Canada.

Contents

List of Figures

List of Tables

Chapter A

Introduction

In the last two decades Nuclear Magnetic Resonance (NMR) spectroscopy has become one of the most powerful techniques to determine molecular structures. NMR spectroscopy deals with the interaction of electromagnetic radiation with nuclear spins placed in a magnetic field. The orientation of the angular momentum vector of a nucleus is quantized with respect to the applied magnetic field. The magnetic field interacts with the local magnetic moment of the nucleus and the resultant interaction energies vary with its different states. The applied radio frequency irradiation excites the nuclei. The response is recorded to get a spectrum. For chemists, it is key that the resonance frequency depends on the electronic and thus, the chemical environment of the nucleus. This effect is called chemical shielding. The diverse resonance frequencies of nuclei in a molecule then can be associated with functional groups. The resonance frequencies are also influenced by neighboring nuclei, which are only a few chemical bonds apart. For different quantum states of the neighboring nucleus, the spins of the binding electrons have different influences to the other nucleus. This indirect coupling, called j-coupling, changes the resonance frequency and splits the recorded line in a characteristic way. Both the chemical shielding and the j-coupling provide much information, which is used to solve the structure

of molecules in the liquid phase.

Solid state NMR spectra are quite different and more complicated. In liquid phase the molecules are moving very quickly in comparison to the NMR time-scale. The measured signals are averaged over all orientations of the molecule. These frequencies are the isotropic resonance frequencies of the nuclei. In the solid state, this motion does not exist or is very slow. NMR resonance frequencies are dependent on the orientation of the molecule in the magnetic field (this is called anisotropy). In addition to j-coupling and chemical shielding there is dipolar coupling. The dipolar coupling results from the through-space interaction of the magnetic moments of different nuclei. Its magnitude depends on the spin types, the distance between the interacting nuclei and the relative orientation of the spins. The fast motion of molecules in the liquid phase averages this interaction to zero.

It is important to note the magnitude of the various interactions. Whereas the dipolar and chemical shielding are in the order of kHz - in the case of ^{13}C for example, j-coupling is in the range of Hz. In liquid phase NMR spectra only the isotropic signals are measured. This normally results in a line width of a few Hz. The spectrum, which is over a range of a few kHz, consists of narrow lines. Solid state spectra, on the other hand, consist of signals which are several kHz broad. A spectrum is typically comprised of one broad band (fig. A.2).

In addition to the previous mentioned interactions, quadrupolar coupling effects are present for spins $> \frac{1}{2}$. In case of a quadrupolar nucleus ($I > \frac{1}{2}$) the positive charge distribution in the nucleus is not spherical (fig. B.1). Also, the nucleus is generally surrounded by an anisotropic distribution of negative electron charge. The resulting interaction energy can be quite large (on the scale of other spin interactions). The resultant "precession" axis is consequently no longer in the direction of the external magnetic field, but along another axis accounting for all large interactions - the Zeeman and quadrupolar which are in the MHz range (fig. B.2). The

electrostatic interaction ranges from weak to dominant in comparison to the Zeeman term. The full range of quadrupole effects can be observed in nature.

1 Magic Angle Spinning in Solid State NMR

Magic Angle Spinning (MAS) is a method to narrow the signals of solid state NMR spectra. Anisotropic interactions such as the dipolar and the chemical shielding interactions can be averaged by macroscopic rotation of the sample about an axis tilted by the magic angle $\theta = \cos^{-1}\sqrt{\frac{1}{3}} = 54.7°$ with respect to the static magnetic field (fig. A.1). Total averaging is only possible, when the spinning frequency is

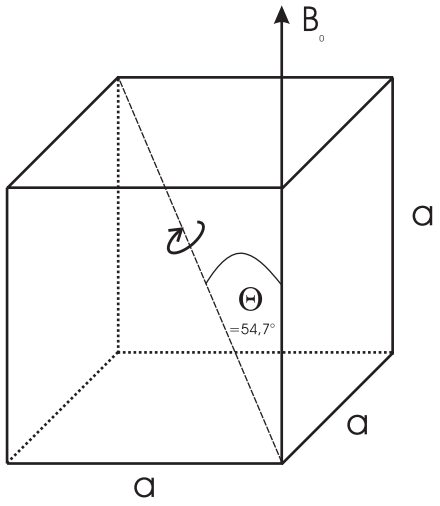

Figure A.1: Schematic structure of the magic angle sample spinning in comparison to the static field. The rotation angle of approximately 54.7° is the angle between the diagonal of a cube and its edges.

larger than the range of the anisotropy - otherwise spinning sidebands appear. Lines recorded with MAS are narrow like the lines of a liquid sample. A comparison between a static solid state spectrum and fast MAS spectrum is given in Figure (A.2). MAS is one of the most important utilities to simplify solid state NMR spectra. Of course, it should be kept in mind, that averaging also results in an

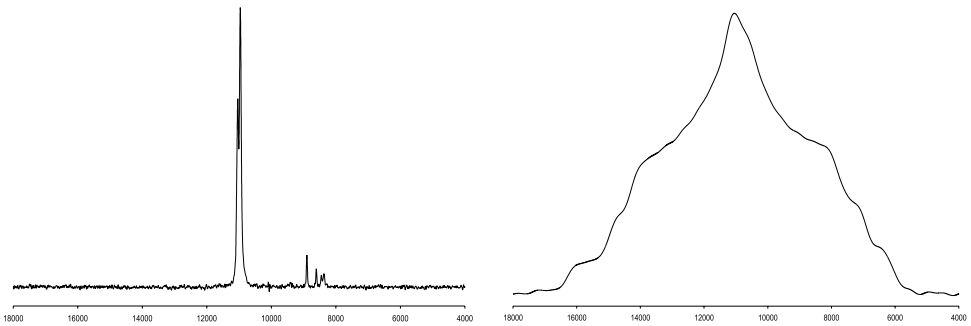

Figure A.2: Solid state NMR spectrum of ^{13}C enriched acetanilide.
left: Spinning about the magic angle at 8054Hz,
right: Static powder pattern

reduction of information about the system. However, information is retained in the spinning side-band pattern.

If a quadrupolar nucleus is coupled to an observed spin-$\frac{1}{2}$ a residual dipolar coupling effect can appear. For quadrupolar nuclei the quantization axis is normally not aligned in the direction of the magnetic field. Spinning of the sample causes a time-dependent change of the molecular orientation with respect to the static magnetic field. Because the electric field gradient (which determines the quadrupolar interaction - it is a measure of electron distribution anisotropy about the nucleus) is fixed in the molecular frame, the alignment of the quantization axis of the quadrupolar nucleus, which combines both effects, electrostatic and magnetic, changes with spinning of the sample. Total averaging of the dipolar coupling with MAS is not possible. The residual influence of the quadrupolar nucleus to the observed nucleus differs for its quantum states m_z. Therefore, in MAS spectra of spin-$\frac{1}{2}$ systems coupled to quadrupolar nuclei, the resonance frequency is split.

2 MAS Spectra Simulations of Quadrupolar Coupled Spin Systems

The simulation of MAS spectra is quite difficult, because the tensors in the Hamiltonian become time-dependent and the time-propagation of the wavefunction gets problematic. In case of slow MAS, the spectrum consists of spinning sidebands (e.g. fig. E.11). The calculation of these sideband intensities, for the simplest case of a one-spin system, was solved in a convenient way by Herzfeld *et al.* [1]. In more general cases the time-dependent Schrödinger equation is not solvable in an analytic way, and approximations have to be considered.

Current available methods to calculate CP/MAS spectra for spin-$\frac{1}{2}$ systems coupled to quadrupolar nuclei use first-order perturbation theory [2, 3, 4, 5]. This approach is valid only for small quadrupolar and/or dipolar couplings, in comparison to the Zeeman term. This approach is very common in studies of the $^{13}C-^{14}N$ spin system. In this case the quadrupolar term is small enough and perturbation theory is usually successful [2, 6, 7, 8, 9]. In other cases these couplings are often too big for quantitative modeling using the perturbation approach.

In cases where the quadrupolar coupling is much bigger than the Zeeman interaction, the latter term can be handled as a perturbation of the quadrupolar interaction. This approach is than called "inverse" perturbation theory. An example of this is the $^{13}C-^{79,81}Br$ system [10]. In contrast, the quadrupolar coupling is in the same range as the Zeeman interaction for the $^{13}C-^{35,37}Cl$ and $^{13}C-^{59}Co$ system [11]. In this case the theoretical description with perturbation theory is not in general valid. Other methods, e.g. polynomial fitting to the exact solution can be necessary [12], or the simulation only of the central band for the fast spinning limit is considered [11]. A general and detailed illustration of the perturbation treatment and its validity is given by Harris *et al.* [4].

Relatively new is the use of Floquet theory for solving the complicated time-dependent equations [13, 14, 15, 16]. In Floquet theory the periodic time alteration of the Hamiltonian is expanded in a Fourier series, which leads to a time-independent formulation involving larger matrices. The problem is, that current Floquet theory is not practical for quadrupolar coupled spin systems, because the matrices arising are often too big and the computation time to diagonalize the large matrices is too long. In the new simulation program, *LanXSSQ*, the large quadrupole and the Zeeman interactions are effectively eliminated via average Hamiltonian theory. The average residual components of the Hamiltonian, and consequently the Liouvillian, are then be handled with Floquet theory.

This project comprises the testing and development of this program, and an investigation of the theory by comparison of computed and experimental data. Different systems are considered, focusing on the case of a spin-$\frac{1}{2}$ nucleus coupled to a quadrupolar nucleus ($I > \frac{1}{2}$). The principle system treated was ^{13}C labeled acetanilide (fig. E.1, page 37), which exhibits residual dipolar coupling to the ^{14}N-spin. The syntheses, X-ray single-crystal structure determination and CP/MAS NMR data, at different B_0-fields, are also presented.

Chapter B

Residual Dipolar Coupling in MAS Spectra

Residual dipolar effects through quadrupolar nuclei occur mainly in solid state NMR spectra, because in liquid phase tumbling of molecules averages the coupling and eliminates it from a recorded spectrum.

Normally, a nucleus is quantized along the applied magnetic field (fig. B.1). In most cases of a quadrupolar nucleus, this is not true. If an electric field gradient is present, the non spherical charge distribution of the quadrupolar nucleus interacts with the electric field gradient. The quadrupolar nucleus is influenced by a magnetic and an electrostatic interaction - the quantization axis is directed in a way which combines both effects (fig. B.2). During MAS the orientation of the molecule changes. Because the electric field gradient is fixed in the molecular frame, the orientation of electric field gradient (electrostatic interaction) to the magnetic field (magnetic interaction) changes with the rotation of the sample. The orientation of the quantization axes of the quadrupolar nucleus thus depend on the relative orientation of the molecule in the magnetic field. In this case, MAS cannot completely average the dipolar coupling to the quadrupolar nucleus.

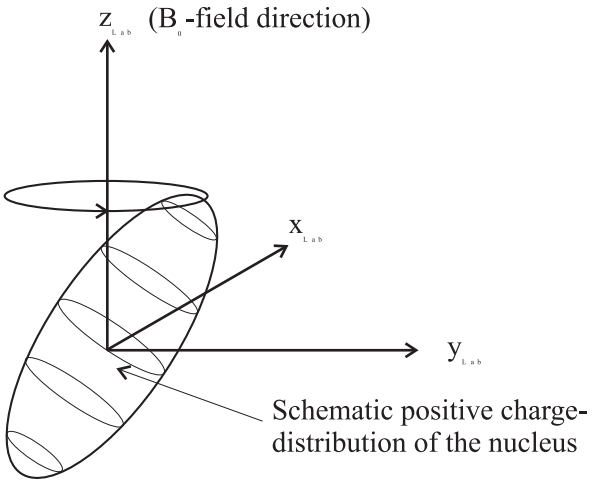

Figure B.1: Schematic structure of a precessing nucleus, with a non-spherical charge distribution, in the magnetic field.

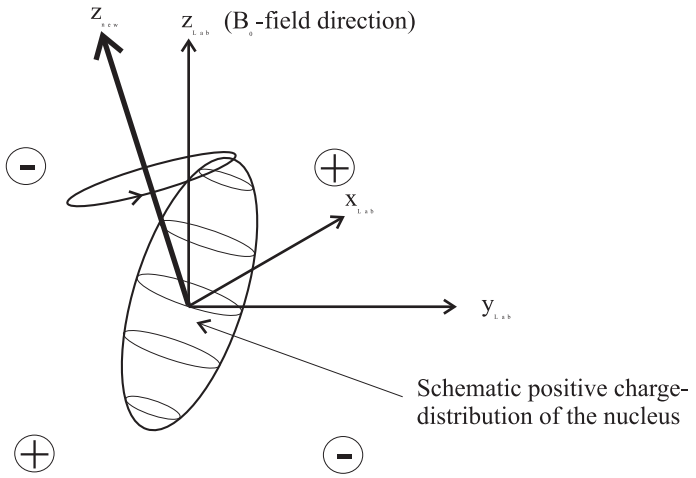

Figure B.2: Schematic structure of a precessing quadrupolar nuclei in a magnetic field, with an electric field gradient present. The quantization axis is now not equivalent to the direction of the magnetic field.

In case of residual dipolar coupling to a quadrupolar nucleus two extremes can be distinguished. In the first case, the electrostatic interaction is small in comparison to the magnetic one (high field approximation) and the quantization axes is almost aligned with the axes of the magnetic field (fig. B.3). In the second case, the magnetic interaction of the quadrupolar nucleus is small in comparison to the electrostatic one and the quantization axis is almost directed along the electric field gradient (fig. B.5). The influence of the quadrupolar nucleus on the observed spin-$\frac{1}{2}$ nucleus causes in the above mentioned cases different splitting and broadening effects of the resonance line. In both cases perturbation theory approaches are useful to explain these coupling effects.

In perturbation theory the first order change in the wavefunction and the second order effect in energy is considered. A good understandable review article about this problem is given by Grondona *et al.* [5]. They treat the electrostatic interaction of the quadrupole nucleus as a perturbation in the case of ^{13}C coupled to ^{14}N. The ^{14}N-nucleus has three different m_z states, m_z=1,0,-1 (see fig. B.3). The quadrupolar coupling constant (electrostatic interaction) is in the range of 3 MHz. The resonance frequency through the influence of a magnetic field varies from 14.4 MHz (4.7 T field strength) to 36.1 MHz (11.75 T field strength), which are the most common field strengths used in modern NMR spectrometers. Here, perturbation theory is a good approximation.

The following equations represent the second order corrected transition frequencies of the spin-$\frac{1}{2}$ nucleus,

$$\nu_{[A]} = \nu_I - D\left(1 - 3\cos^2\xi\right) - \frac{9D\chi}{4\nu_S}\sin^2\xi\cos^2\xi \tag{B.1}$$

$$\nu_{[B]} = \nu_I + \frac{9D\chi}{2\nu_S}\sin^2\xi\cos^2\xi \tag{B.2}$$

$$\nu_{[C]} = \nu_I + D\left(1 - 3\cos^2\xi\right) - \frac{9D\chi}{4\nu_S}\sin^2\xi\cos^2\xi \tag{B.3}$$

where ξ gives the orientation of the dipolar vector relative to the magnetic field

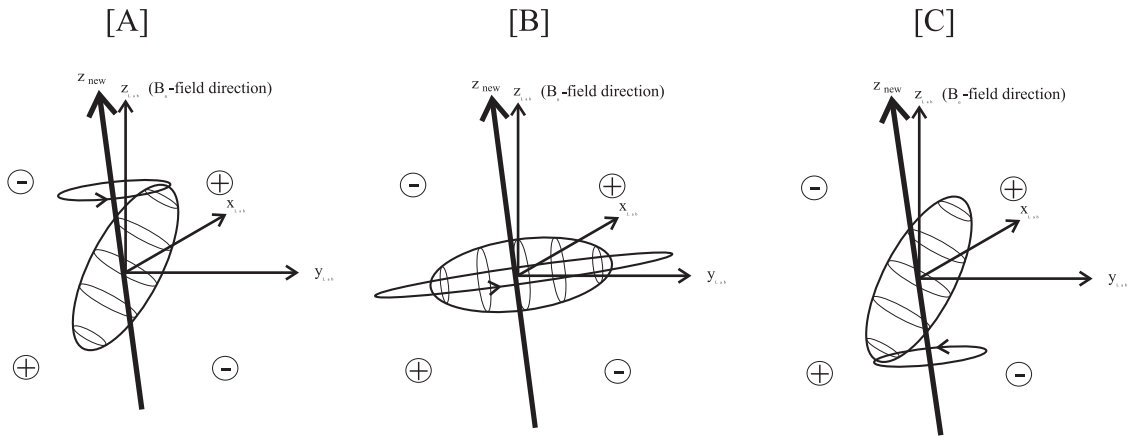

Figure B.3: Schematic presentation of the three orientations of a spin one nucleus in the magnetic field under influence of a weak electric field gradient.
Figure [A]: $m_{z_{new}}$=1, [B]: $m_{z_{new}}$=0, [C]: $m_{z_{new}}$=-1

direction. The static single crystal spectrum of the spin-$\frac{1}{2}$ nucleus is a 1 : 1 : 1 triplet according to the frequencies in equation (B.1 - B.3).

In MAS, ξ is time-dependent and an averaging procedure is necessary to get the resultant time-independent frequencies. The averaged transition frequencies,

$$\nu_{[A]} = \nu_I + \frac{D\chi}{\nu_S}\left(-\frac{3}{8} + \frac{3}{4}\cos^2\Theta - \frac{7}{8}\cos^4\Theta\right) \quad \text{(B.4)}$$

$$\nu_{[B]} = \nu_I + \frac{D\chi}{\nu_S}\left(\frac{3}{4} - \frac{3}{2}\cos^2\Theta + \frac{7}{4}\cos^4\Theta\right) \quad \text{(B.5)}$$

$$\nu_{[C]} = \nu_I + \frac{D\chi}{\nu_S}\left(-\frac{3}{8} + \frac{3}{4}\cos^2\Theta - \frac{7}{8}\cos^4\Theta\right) \quad \text{(B.6)}$$

now depend on the relative orientation, Θ, of the dipolar axis with respect to the spinning axes. With MAS, the angle dependent dipolar term $[D\,(1 - 3\cos^2\xi)]$ of equations (B.1) and (B.3) is averaged to zero. The resonance frequencies $\nu_{[A]}$ and $\nu_{[B]}$ become equivalent. The spectrum consists of two lines, with relative intensity 2:1. Diagram (B.4) shows the energy levels of a spin-$\frac{1}{2}$ coupled to a quadrupolar nucleus (spin-1). The outer levels include only the Zeeman interactions of the two spin system. The middle levels include the quadrupolar interaction, while the inner

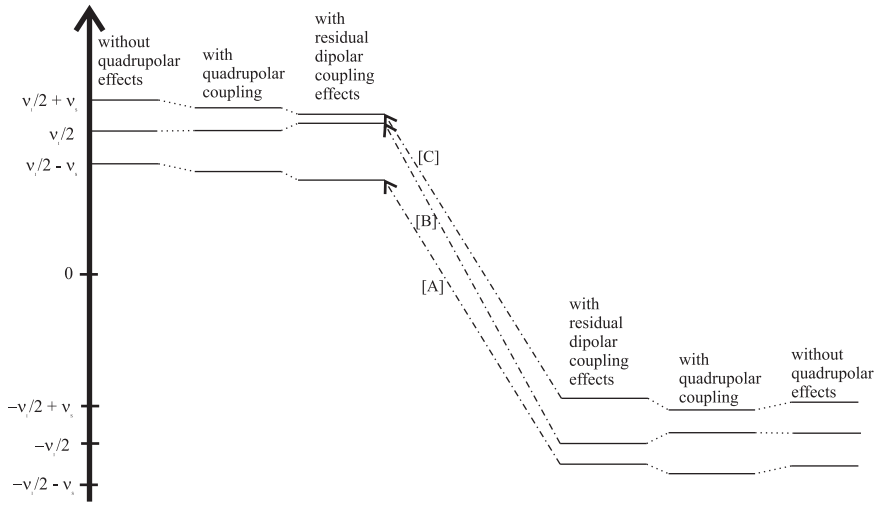

Figure B.4: Schematic presentation of the energy levels of a two spin system, ^{13}C coupled to ^{14}N. The changes in energy levels due to residual dipolar coupling are exagerated!

levels also include the residual dipolar interaction to the spin-$\frac{1}{2}$ nucleus under MAS condition. The three transition frequencies of the spin-$\frac{1}{2}$ nucleus are denoted with dotted arrows. MAS averages these transitions about the sample spinning axis. The remaining of the frequencies results in Pake pattern for the two observed lines. However, this effect is small compared with the splitting of the lines and is observed as line-broadening patterns.

In case of strong quadrupolar coupling, the electrostatic interaction is much larger than the magnetic interaction and the quantization axis is almost in the direction of the electric field gradient (fig. B.5). A good example is the residual dipolar coupling between ^{79,81}Br and ^{13}C. This system is described with "inverse" perturbation theory, wherein the magnetic interaction is handled as a perturbation of the electrostatic interaction [10, 17]. In the MAS spectrum, the residual dipolar coupling is again averaged about the sample spinning axis. The remaining orientation dependence again results in Pake patterns. But like the case of weak quadrupolar interaction, the frequencies only vary a little with orientation and one only observed

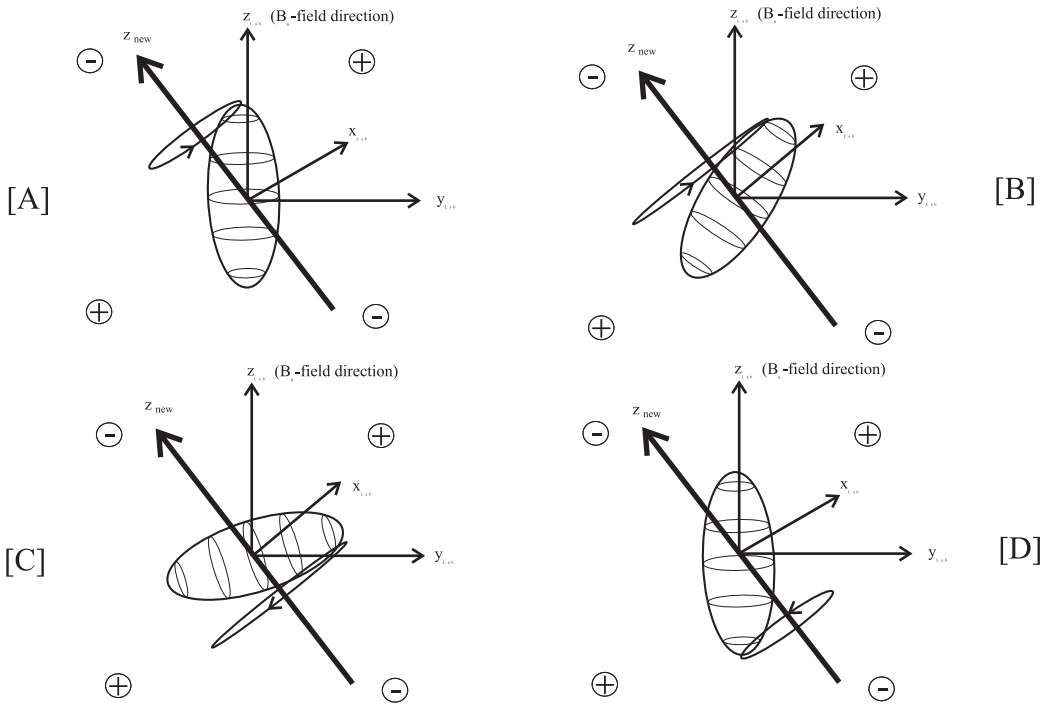

Figure B.5: Schematic presentation of the four orientations of a spin-$\frac{3}{2}$ nucleus in the magnetic field under influence of a strong electric field gradient.

Figure [A]: $m_{z_{new}}=\frac{3}{2}$, [B]: $m_{z_{new}}=\frac{1}{2}$, [C]: $m_{z_{new}}=-\frac{1}{2}$, [D]: $m_{z_{new}}=-\frac{3}{2}$

broadened lines. Note, that in the case of large quadrupolar coupling there are distinct lines for each state of the quadrupolar nucleus.

If the quadrupolar interaction is comparable to the Zeeman interaction, the spectra are more complicated. In the case of ^{35,37}Cl coupling to ^{13}C this situation is present at magnetic fields around 4.7 T [18]. The basic four resonance frequencies are still present, but the orientation dependence of the frequencies is larger and also the splitting of these lines can be smaller and resulting Pake patterns can overlap. In experimental MAS spectra, Pake patterns are visible. Simulation of this spectra requires numerical calculation of the Zeeman-quadrupolar eigenvalues and eigenvectors - also, further assumptions are needed [18, 19].

We have considered three different magnitudes of quadrupolar interaction. For each case different treatments and therefore different simulation programs are required. We wish to solve the problem more generally. The resulting simulation program uses complete theory permitting simulation of spectra for all three cases.

Chapter C

Theoretical Overview

In quantum mechanics the time-evolution of an ensemble of nuclei is described with the Liouville von Neuman equation (density matrix formulation of quantum mechanics),

$$\hat{\hat{\mathcal{L}}}\rho = i\hbar\frac{\partial\rho}{\partial t} \tag{C.1}$$

which is the generalization of the time-dependent Schrödinger equation. $\hat{\hat{\mathcal{L}}}$, the Liouvillian, is defined as $[\hat{\mathcal{H}}, \square]$ and ρ represents the density matrix. The use of the Liouville von Neumann equation is necessary, if (differential) relaxation and/or chemical exchange effects are important. Its formal solution can be written as in equation (C.2).

$$\rho(t) = \hat{T}\, e^{-i\int_0^t \mathrm{d}t' \hat{\hat{\mathcal{L}}}(t')}\, \rho(0) \tag{C.2}$$

The calculation of the propagator $\mathbf{U}(t) = e^{-i\int_0^t \mathrm{d}t' \hat{\hat{\mathcal{L}}}(t')}$ is not trivial, because in the case of spinning, $\hat{\hat{\mathcal{L}}}$ itself is time-dependent. Generally the Liouvillian for different times does not commute with itself,

$$\left[\hat{\hat{\mathcal{L}}}(t_1),\, \hat{\hat{\mathcal{L}}}(t_2)\right] \neq 0 \tag{C.3}$$

which causes the need of the time-ordered exponential function. This is expressed in equation (C.2) with the time-ordering operator $\hat{T}$. Details about the time-ordered exponential function are given in reference [20]. If the evolution of the density matrix is known, the spectrum can be calculated according to equation (C.4), where $\mathcal{F}[f(t)]$ is fourier-transformed $f(t)$ and $\mathrm{d}^\dagger$ is the detector operator (i.e. $\hat{\mathrm{I}}_x$ or $\hat{\mathrm{I}}_y$).

$$\begin{aligned} \text{spectrum}(\nu) &= \mathrm{d}^\dagger \, \mathcal{F}\left[\rho(t)\right] \\ &= \mathrm{d}^\dagger \int_0^\infty \mathrm{d}t \, e^{i\nu t} \rho(t) \end{aligned} \tag{C.4}$$

In the case of a spin-$\frac{1}{2}$ coupled to a spin $I > \frac{1}{2}$, the Hamiltonian consists of the terms,

$$\hat{\mathcal{H}} = \hat{\mathcal{H}}_Z + \hat{\mathcal{H}}_\sigma + \hat{\mathcal{H}}_J + \hat{\mathcal{H}}_D + \hat{\mathcal{H}}_Q \tag{C.5}$$

whereas $\hat{\mathcal{H}}_Z$ represents the magnetic interaction of the nuclei (Zeeman interaction), $\hat{\mathcal{H}}_\sigma$ the chemical shielding terms, $\hat{\mathcal{H}}_J$ the j-coupling, $\hat{\mathcal{H}}_D$ the dipolar coupling and $\hat{\mathcal{H}}_Q$ the quadrupolar coupling. This Hamiltonian expressed in terms of angular momentum operators has the form,

$$\begin{aligned} \hat{\mathcal{H}} &= \boldsymbol{B}^T(\gamma_I \hat{I} + \gamma_S \hat{S}) - \boldsymbol{B}^T(\gamma_I \boldsymbol{\sigma_I} \hat{I} + \gamma_S \boldsymbol{\sigma_S} \hat{S}) + \\ &\quad \hat{I}^T \boldsymbol{J} \hat{S} + \hat{I}^T \boldsymbol{D} \hat{S} + \hat{S}^T \boldsymbol{Q} \hat{S} \end{aligned} \tag{C.6}$$

with the angular momentum operators

$$\hat{I} = \begin{pmatrix} \frac{I_+ + I_-}{2} \\ \frac{I_+ - I_-}{2i} \\ I_z \end{pmatrix} \tag{C.7}$$

and

$$\hat{S} = \begin{pmatrix} \frac{S_+ + S_-}{2} \\ \frac{S_+ - S_-}{2i} \\ S_z \end{pmatrix} \tag{C.8}$$

of the spin-$\frac{1}{2}$ and quadrupolar nuclei respectively. The x and y components of the angular momentum operators are expressed in terms of raising (I_+, S_+) and lowering operators (I_-, S_-). The tensors $\boldsymbol{\sigma}$, $\boldsymbol{J}$, $\boldsymbol{D}$ and $\boldsymbol{Q}$ correspond to the previous mentioned interactions in the Hamiltonian (C.5). The magnetic field vector is declared with $\boldsymbol{B}$ (in this case the magnetic field is aligned with the z-axis of the coordinate system) and $\gamma_{I,S}$ is the magnetogyric ratio of the corresponding nucleus.

Spinning causes the time-dependent change of the molecular orientation in the magnetic field. This results in a time-dependence of the tensors $\boldsymbol{\sigma}$, $\boldsymbol{J}$, $\boldsymbol{D}$ and $\boldsymbol{Q}$ in equation (C.6). Therefore the Hamiltonian and consequently the Liouvillian are time dependent. The time alteration is described with Floquet theory to solve equation (C.1).

In case of quadrupolar coupling many Floquet blocks[1] would be needed to converge a spectrum and the size of arising matrices is too large for spectra calculations. To reduce the number of Floquet blocks, the large quadrupolar and Zeeman term have to be incorporated via average Hamiltonian theory. This reduces the spectral range, which is connected with the number of Floquet blocks needed to converge the simulated spectrum (see eq. C.44).

1 Average Hamiltonian Theory

In the description of the time-evolution of quantum systems, such as spin systems, the Hamiltionian consists of parts with different time-scales. In our case the time-scale of the Zeeman and the quadrupolar terms are in the range of MHz. On the other hand, the dipolar coupling and chemical shielding parts are roughly three orders of magnitude slower. In average Hamiltonian theory the dominant fast part can average a part of the slower Hamiltonian to zero - the slow Hamiltonian is truncated. The averaged slow Hamiltionian is constructed as follows:

[1] The definition of a Floquet block is given on page 23

The formal solution of the time-dependent Schrödinger equation[2],

$$\hat{\mathcal{H}}\Psi = i\frac{\partial\psi}{\partial t} \tag{C.9}$$

is given by

$$\Psi(t) = \hat{T}\, e^{-i\int_0^t \hat{\mathcal{H}}\mathrm{d}t'}\Psi(0). \tag{C.10}$$

Suppose the Hamiltonian consists of two different parts (see section 3),

$$\hat{\mathcal{H}} = \hat{\mathcal{H}}_F + \hat{\mathcal{H}}_S \tag{C.11}$$

which are distinguished in their energy spacing. The energy spacing of $\hat{\mathcal{H}}_F$ is much bigger than that of $\hat{\mathcal{H}}_S$. This results in fast time evolution due to $\hat{\mathcal{H}}_F$ in conjunction with a slower evolution due to $\hat{\mathcal{H}}_S$. $\hat{\mathcal{H}}_F$ represents the quadrupolar coupling and the Zeeman term. $\hat{\mathcal{H}}_S$ consists the chemical shielding, the J coupling and the dipolar coupling term. Combination of (C.11) and (C.10) results in

$$\Psi(t) = \hat{T}\, e^{-i\int_0^t (\hat{\mathcal{H}}_F+\hat{\mathcal{H}}_S)\mathrm{d}t'}\Psi(0) \tag{C.12}$$

we let

$$\phi(t) = e^{i\hat{\mathcal{H}}_F t}\Psi(t) \tag{C.13}$$

with the aim of removing the fast Hamiltonian. Here, we neglect the time-dependence of $\hat{\mathcal{H}}_F$. This will be addressed below. Now the time evolution of $\phi(t)$ is calculated.

Differentiation of equation (C.13) and use of the Schrödinger-equation (C.9) results in (we can assume a time-independent $\hat{\mathcal{H}}_F$ because we consider a time-propagation which is small compared with sample spinning, but large compared

[2]In all following equations $\hbar$ is set to one.

with the quadrupolar spin dynamics)

$$\begin{aligned}\frac{\partial}{\partial t}\phi(t) &= e^{i\hat{\mathcal{H}}_F t} i\hat{\mathcal{H}}_F \Psi + e^{i\hat{\mathcal{H}}_F t}\frac{\partial \Psi}{\partial t} \\ &= e^{i\hat{\mathcal{H}}_F t}[i\hat{\mathcal{H}}_F \Psi + \frac{\partial \Psi}{\partial t}] \\ &= e^{i\hat{\mathcal{H}}_F t}[i\hat{\mathcal{H}}_F \Psi - i\hat{\mathcal{H}}\Psi] \\ &= ie^{i\hat{\mathcal{H}}_F t}[\hat{\mathcal{H}}_F \Psi - \hat{\mathcal{H}}\Psi] \\ &= ie^{i\hat{\mathcal{H}}_F t}[\hat{\mathcal{H}}_F - \hat{\mathcal{H}}]\Psi \\ &= -ie^{i\hat{\mathcal{H}}_F t}\hat{\mathcal{H}}_S \Psi\end{aligned} \tag{C.14}$$

From substitution of equation (C.13) in equation (C.14) follows

$$i\frac{\partial}{\partial t}\phi(t) = e^{i\hat{\mathcal{H}}_F t}\hat{\mathcal{H}}_S e^{-i\hat{\mathcal{H}}_F t}\phi(t) \tag{C.15}$$

Integration of equation (C.15), inserting with $\sum_{E_F} |E_F\rangle \langle E_F| = 1$, and substituting

$$\phi(t') = \sum_{E'_F} C_{E'_F}(t') |E'_F\rangle , \tag{C.16}$$

results in

$$\begin{aligned}i[\phi(t) - \phi(0)] &= \int_0^t \mathrm{d}t'\, e^{i\hat{\mathcal{H}}_F t'} \\ &\quad \sum_{E_F} \Big(|E_F\rangle \langle E_F| \Big) \hat{\mathcal{H}}_S e^{-i\hat{\mathcal{H}}_F t'} \sum_{E'_F} C_{E'_F}(t') |E'_F\rangle\end{aligned} \tag{C.17}$$

With use of the spectral theorem [21]

$$f(\hat{\mathcal{H}}_F)|E_F\rangle = f(E_F)|E_F\rangle , \quad \text{where} \quad \hat{\mathcal{H}}_F |E_F\rangle = E_F |E_F\rangle , \tag{C.18}$$

and definitions of equation (C.16) follows,[3]

$$\begin{aligned}\sum_{E_F} C_{E_F}(t)|E_F\rangle &= \sum_{E_F} C_{E_F}(0)|E_F\rangle - i \sum_{E_F,\, E'_F} \int_0^t \mathrm{d}t' \\ &\quad e^{i(E_F - E'_F)t'} \langle E_F| \hat{\mathcal{H}}_S |E'_F\rangle C_{E'_F}(t')|E_F\rangle\end{aligned} \tag{C.19}$$

[3] remember: $\langle E_F| \hat{\mathcal{H}}_S |E_F\rangle$ is only a scalar. It is thus possible to change the arrangement of $|E_F\rangle$

Because the coefficients are unique, we must have

$$\begin{aligned} C_{E_F}(t) &= C_{E_F}(0) \\ &\quad -i\sum_{E'_F}\int_0^t \mathrm{d}t'\, e^{i(E_F-E'_F)t'}\ \langle E_F|\,\hat{\mathcal{H}}_S\,|E'_F\rangle\ C_{E'_F}(t') \end{aligned} \tag{C.20}$$

The integration over time, t, is split into a sum of integrations over a short time, τ;

$$t = N\tau \tag{C.21}$$

τ is chosen to be short on the $\hat{\mathcal{H}}_S$ time scale, but long on the $\hat{\mathcal{H}}_F$ time scale. The integral is expressed as

$$\begin{aligned} &\sum_{n=1}^{N}\int_{(n-1)\tau}^{n\tau} \mathrm{d}t'\, e^{i(E_F-E'_F)t'}\ \hat{\mathcal{H}}_{S,\,E_F,\,E'_F}\, C_{E'_F}(t') \\ \cong\ &\sum_{n=1}^{N} C_{E'_F}((n+\frac{1}{2})\,\tau)\ \ \hat{\mathcal{H}}_{S,E_F,E'_F}\int_{(n-1)\tau}^{n\tau} \mathrm{d}t'\, e^{i\left(E_F-E'_F\right)t'} \end{aligned} \tag{C.22}$$

We distinguish two cases of the integral in equation (C.19): first, $E_F = E'_F$ and second $E_F \neq E'_F$. In the second case, we have

$$\cong \sum_{n=1}^{N} C_{E'_F}((n+\frac{1}{2})\,\tau)\ \ \hat{\mathcal{H}}_{S,\,E_F,\,E'_F}\left(\frac{e^{i(E_F-E'_F)t'}}{i(E_F-E'_F)}\right)\Bigg|_{(n-1)\tau}^{n\tau} \tag{C.23}$$

which is small because of the $E_F - E'_F$ denominator (large energy splitting of the $\hat{\mathcal{H}}_F$ eigenstates is assumed). We neglect these terms on this account. For the remaining terms, with $E_F = E'_F$, the integral is given by

$$\cong \sum_{n=1}^{N} C_{E'_F\,(n\tau)}\hat{\mathcal{H}}_{S,\,E_F,\,E'_F}\,\tau \tag{C.24}$$

and both cases combined results in,

$$\cong \int_0^t \mathrm{d}t'\, C_{E'_F}(t')\hat{\mathcal{H}}_{S,\,E_F,\,E'_F}\,\delta_{E_F,E'_F}. \tag{C.25}$$

In the last step the sum is changed back to the integration, but now with the separation of time scales invoked (i.e. neglecting $(E_F - E'_F)^{-1}$ terms). With combination of the remaining parts of equation (C.25) and equation (C.19), follows

$$C_{E_F}(t) \cong C_{E_F}(0) - i \int_0^t \mathrm{d}t' \, C_{E_F}(t') \hat{\mathcal{H}}_{S,\,E_F,\,E_F} \tag{C.26}$$

For simplicity, we neglect the possibility of degeneracy of eigenvalues, E_F. This possibility is easily included in the final result. The formalism is correct for all coefficients in the wavefunction $\phi(t)$. Equation (C.16) gives the complete wavefunction.

$$\sum_{E_F} C_{E_F}(t) \left|E_F\right\rangle \cong \sum_{E_F} \left[C_{E_F}(0) - i \int_0^t \mathrm{d}t' \left\langle E_F\right| \hat{\mathcal{H}}_S \left|E_F\right\rangle C_{E_F}(t') \right] \left|E_F\right\rangle \tag{C.27}$$

$$\begin{aligned}
\phi_F(t) - \phi_F(0) &\cong -i \int_0^t \mathrm{d}t' \, \left[\left\langle E_F\right| \hat{\mathcal{H}}_S \left|E_F\right\rangle \right] \phi_F(t') \\
\mathrm{d}\phi_F(t) &\cong -i\mathrm{d}t \, \left[\left\langle E_F\right| \hat{\mathcal{H}}_S \left|E_F\right\rangle \right] \phi_F(t) \\
i \frac{\partial}{\partial t} \phi_F(t) &\cong \left[\left\langle E_F\right| \hat{\mathcal{H}}_S \left|E_F\right\rangle \right] \phi_F(t) \\
i \frac{\partial}{\partial t} \phi_F(t) &\cong \overline{\hat{\mathcal{H}}_S} \phi_F(t)
\end{aligned} \tag{C.28}$$

$\left[\left\langle E_F\right| \hat{\mathcal{H}}_S \left|E_F\right\rangle \right]$ is the matrix consisting only of the diagonal components of $\overline{\hat{\mathcal{H}}_S}$ in the $\hat{\mathcal{H}}_F$-representation. The resulting $\overline{\hat{\mathcal{H}}_S}$ commutes with $\hat{\mathcal{H}}_F$. This average Hamiltonian is easily constructed - with $\hat{\mathcal{H}}_S$ expressed in the $\hat{\mathcal{H}}_F$ eigen-representation - by dropping all terms in the slow Hamiltonian matrix which correspond to distinct eigenvalues for $\hat{\mathcal{H}}_F$. The principle is illustrated in equation (C.29). The terms marked with boxes, are cross terms connecting eigenstates of $\hat{\mathcal{H}}_F$ associated with distinct eigenvalues, E_k and E_l. They are be dropped to form $\overline{\hat{\mathcal{H}}_S}$ in the $\hat{\mathcal{H}}_F$ repre-

sentation.

$$\overline{\hat{\mathcal{H}}}_S = \begin{pmatrix} \ddots & \ddots & \ddots & \ddots & \ddots \\ \ddots & \left\langle \Psi_n^{E_k} \middle| \hat{\mathcal{H}}_S \middle| \Psi_n^{E_k} \right\rangle & \boxed{\left\langle \Psi_n^{E_k} \middle| \hat{\mathcal{H}}_S \middle| \Psi_{n+1}^{E_l} \right\rangle} & \left\langle \Psi_n^{E_k} \middle| \hat{\mathcal{H}}_S \middle| \Psi_{n+2}^{E_k} \right\rangle & \ddots \\ \ddots & \boxed{\left\langle \Psi_{n+1}^{E_l} \middle| \hat{\mathcal{H}}_S \middle| \Psi_n^{E_k} \right\rangle} & \left\langle \Psi_{n+1}^{E_l} \middle| \hat{\mathcal{H}}_S \middle| \Psi_{n+1}^{E_l} \right\rangle & \boxed{\left\langle \Psi_{n+1}^{E_l} \middle| \hat{\mathcal{H}}_S \middle| \Psi_{n+2}^{E_k} \right\rangle} & \ddots \\ \ddots & \left\langle \Psi_{n+2}^{E_k} \middle| \hat{\mathcal{H}}_S \middle| \Psi_n^{E_k} \right\rangle & \boxed{\left\langle \Psi_{n+2}^{E_k} \middle| \hat{\mathcal{H}}_S \middle| \Psi_{n+1}^{E_l} \right\rangle} & \left\langle \Psi_{n+2}^{E_k} \middle| \hat{\mathcal{H}}_S \middle| \Psi_{n+2}^{E_k} \right\rangle & \ddots \\ \ddots & \ddots & \ddots & \ddots & \ddots \end{pmatrix} \tag{C.29}$$

This action block-diagonalizes the Hamiltonian.

Equation (C.23) and (C.24) show that the average Hamiltonian theory is valid when the energy differences associated with $\hat{\mathcal{H}}_F$ are much larger than those of $\hat{\mathcal{H}}_S$. If no quadrupolar nuclei are present, the Zeeman interaction is the fast Hamiltonian. It is generally more than 3 orders of magnitude faster than all other interactions in such cases.

2 Floquet Theory

In simulations of MAS, the tensors in the Hamiltonian change with time. The sample spins about a fixed axis resulting in periodic time-dependent tensors. This periodicity can be exploited to get an useful expression for the density-matrix propagator.

Sample spinning results in a periodic average Hamiltonian (a 5 term series in the case of no quadrupolar nuclei [16]) and Liouvillian, which we express in a Fourier series:

$$\hat{\hat{\mathcal{L}}}(t) = \sum_{j=-n}^{n} \hat{\hat{\mathcal{L}}}^{(j)} e^{ij\omega t} \tag{C.30}$$

In practice, this Fourier series is determined by computing the average Hamiltonian for many rotor phases and inverse Fourier transforming (on an element by element basis). Note that use of the average Hamiltonian for each rotor phase is permitted only if the fast Hamiltonian is much faster than the sample spinning. This is why we can neglect the time-dependence (due to sample spinning) of $\hat{\mathcal{H}}_F$ in section (1).

$$\hat{\hat{\mathcal{L}}}^{(j)} = \left[\hat{\mathcal{H}}^{(j)}, \square\right], \tag{C.31}$$

where $\hat{\mathcal{H}}^{(j)}$ is the resulting jth Fourier component of $\overline{\hat{\mathcal{H}}}_S$. The propagator associated with $\hat{\hat{\mathcal{L}}}(t)$ can be written as a Fourier-like series where the coefficients are themselves time-dependent.

$$\mathbf{U}(t) = \sum_{k=-\infty}^{\infty} \mathbf{U}^{(k)}(t)\, e^{ik\omega t} \tag{C.32}$$

Substitution of the definition of the propagator in equation (C.2) shows, that the propagator must satisfy the Liouville von Neuman equation.

$$\frac{\partial}{\partial t}\mathbf{U}(t) = -i\hat{\hat{\mathcal{L}}}(t)\mathbf{U}(t) \tag{C.33}$$

Combination of equation (C.30) and equation (C.32) with equation (C.33) results in

$$\sum_{k=-\infty}^{\infty} \frac{\partial}{\partial t}\left(\mathbf{U}^{(k)}(t)e^{ik\omega t}\right) = -i\sum_{j=-n}^{n}\sum_{k=-\infty}^{\infty} \hat{\hat{\mathcal{L}}}^{(j)}\mathbf{U}^{(k)}(t)e^{i(j+k)\omega t} \tag{C.34}$$

Taking the derivative on the left, and re-arranging, gives equation (C.35), in which $\delta_{j,0}$ is the Kronecker delta and $\mathbf{1}$ is the unit matrix.

$$\sum_{k=-\infty}^{\infty} e^{ik\omega t}\left(\frac{\partial}{\partial t}\mathbf{U}^{(k)}(t)\right) = -i\sum_{j=-n}^{n}\sum_{k=-\infty}^{\infty}\left(\hat{\hat{\mathcal{L}}}^{(j)} + k\omega\delta_{j,0}\mathbf{1}\right)\mathbf{U}^{(k)}(t)e^{i(j+k)\omega t} \tag{C.35}$$

The k index on the left is arbitrary, so equation (C.35) can be re-written as equation (C.36).

$$\sum_{k=-\infty}^{\infty} e^{ik\omega t}\left(\frac{\partial}{\partial t}\mathbf{U}^{(k)}(t)\right) = -i\sum_{j=-n}^{n}\sum_{k=-\infty}^{\infty}\left(\hat{\hat{\mathcal{L}}}^{(j)} + (k-j)\omega\delta_{j,0}\mathbf{1}\right)\mathbf{U}^{(k-j)}(t)e^{ik\omega t} \tag{C.36}$$

The solution to this equation is unique, so it is satisfied by the solutions of equation (C.37), for all values of k.

$$\frac{\partial}{\partial t}\mathbf{U}^{(k)}(t) = -i\sum_{j=-n}^{n}\left(\hat{\hat{\mathcal{L}}}^{(j)} + (k-j)\omega\delta_{j,0}\mathbf{1}\right)\mathbf{U}^{(k-j)}(t) \tag{C.37}$$

With the definitions of the Floquet Liouvillian matrix,[4]

$$\mathbb{L} = \begin{pmatrix}
\ddots & \ddots & \ddots & \ddots & \ddots & \ddots & \ddots \\
\ddots & \hat{\hat{\mathcal{L}}}^{(n-2)} & \hat{\hat{\mathcal{L}}}^{(n-1)} & \hat{\hat{\mathcal{L}}}^{(n)} & 0 & 0 & \ddots \\
\ddots & \ddots & \ddots & \ddots & \ddots & \ddots & \ddots \\
\ddots & \hat{\hat{\mathcal{L}}}^{(0)} + 2\omega & \hat{\hat{\mathcal{L}}}^{(1)} & \hat{\hat{\mathcal{L}}}^{(2)} & \hat{\hat{\mathcal{L}}}^{(3)} & \hat{\hat{\mathcal{L}}}^{(4)} & \ddots \\
\ddots & \hat{\hat{\mathcal{L}}}^{(-1)} & \hat{\hat{\mathcal{L}}}^{(0)} + \omega & \hat{\hat{\mathcal{L}}}^{(1)} & \hat{\hat{\mathcal{L}}}^{(2)} & \hat{\hat{\mathcal{L}}}^{(3)} & \ddots \\
\ddots & \hat{\hat{\mathcal{L}}}^{(-2)} & \hat{\hat{\mathcal{L}}}^{(-1)} & \hat{\hat{\mathcal{L}}}^{(0)} & \hat{\hat{\mathcal{L}}}^{(1)} & \hat{\hat{\mathcal{L}}}^{(2)} & \ddots \\
\ddots & \hat{\hat{\mathcal{L}}}^{(-3)} & \hat{\hat{\mathcal{L}}}^{(-2)} & \hat{\hat{\mathcal{L}}}^{(-1)} & \hat{\hat{\mathcal{L}}}^{(0)} - \omega & \hat{\hat{\mathcal{L}}}^{(1)} & \ddots \\
\ddots & \hat{\hat{\mathcal{L}}}^{(-4)} & \hat{\hat{\mathcal{L}}}^{(-3)} & \hat{\hat{\mathcal{L}}}^{(-2)} & \hat{\hat{\mathcal{L}}}^{(-1)} & \hat{\hat{\mathcal{L}}}^{(0)} - 2\omega & \ddots \\
\ddots & \ddots & \ddots & \ddots & \ddots & \ddots & \ddots \\
\ddots & 0 & 0 & \hat{\hat{\mathcal{L}}}^{(-n)} & \hat{\hat{\mathcal{L}}}^{(-n+1)} & \hat{\hat{\mathcal{L}}}^{(-n+2)} & \ddots \\
\ddots & \ddots & \ddots & \ddots & \ddots & \ddots & \ddots
\end{pmatrix}, \tag{C.38}$$

[4]The number of Floquet blocks correspond to the block order of the used Floquet Liouvillian matrix (remember: each written element $\hat{\hat{\mathcal{L}}}^{(n)}$ is itself a matrix).

and the propagator matrix

$$\mathbb{U}(t) = \begin{pmatrix} \vdots \\ \mathbf{U}^{(2)}(t) \\ \mathbf{U}^{(1)}(t) \\ \mathbf{U}^{(0)}(t) \\ \mathbf{U}^{(-1)}(t) \\ \mathbf{U}^{(-2)}(t) \\ \vdots \end{pmatrix}, \tag{C.39}$$

the differential propagator equation can be written in a compact matrix form, which is shown in (C.40).

$$i\frac{\partial}{\partial t}\mathbb{U}(t) = \mathbb{L}\mathbb{U}(t) \tag{C.40}$$

The advantage of this formulation is a time-independent Floquet Liouvillian. Equation (C.40) is easily solved to give (C.41).

$$\mathbb{U}(t) = e^{-i\mathbb{L}t}\,\mathbb{U}(0) \tag{C.41}$$

Because at $t = 0$ no propagation has been occurred, $\mathbb{U}(0)$ is the identity operator, and $\mathbf{U}^{(j)}(0) = \mathbf{1}\delta_{j,0}$. The elements of the propagator matrix are given by

$$\mathbf{U}^{(j)}(t) = \left[e^{-i\mathbb{L}t}\right]_{j,k=0} \tag{C.42}$$

The expression for the time-dependent propagator-coefficient in equation (C.42) is substituted in equation (C.32) to determine the propagator in equation (C.2). The combined equations give, after analytical powder averaging and use of the relation in equation (C.4), an expression for the spectrum, which is shown in equation (C.43) [16].

$$\text{spectrum}(\nu) = \mathrm{d}^\dagger \left[\frac{1}{i(2\pi\nu\mathbf{1} + j\omega\mathbf{1} - \mathbb{L})}\right]_{j=0,k=0} \rho(0) \tag{C.43}$$

The matrix $\mathbb{L}$ is infinite in its dimension, but it can be truncated without an apparent effect in the calculated spectrum. To solve equation (C.43) the huge Floquet matrix $\mathbb{L}$ is tridiagonalized with the dual Lanzcos method. Then, the system of equations is solved with linear decomposition [22]. The number of Floquet-blocks (N_F) needed to converge a spectrum is roughly given by,

$$N_F = \frac{2\ (\text{spectral range})}{\nu_R} \tag{C.44}$$

where $\nu_R = \frac{\omega}{2\pi}$ is the rotor frequency.

3 Average Hamiltonian Approach in *LanXSSQ* and its Implementation in Floquet Theory

In MAS experiments, the orientation of a molecule varies with time, which causes the time-dependence of the Hamiltonian. To calculate the spectrum, we need a time-dependent expression of the Hamiltonian. In case of sample spinning, each time is associated with a rotor phase of the spinner. The time-dependence of the rotor phase γ_R is given by,

$$\gamma_R = 2\pi\nu_R t \tag{C.45}$$

whereas ν_R is the spinning frequency and t the time. To get a time series of the averaged slow Hamiltonian, it is calculated for a suitable number of rotor phases.

To use average Hamiltonian theory, the complete Hamiltonian is partitioned into a fast and a slow part,

$$\begin{aligned} \hat{\mathcal{H}} &= \hat{\mathcal{H}}_Z + \hat{\mathcal{H}}_\sigma + \hat{\mathcal{H}}_J + \hat{\mathcal{H}}_D + \hat{\mathcal{H}}_Q \\ \hat{\mathcal{H}} &= \hat{\mathcal{H}}_F + \hat{\mathcal{H}}_S \end{aligned} \tag{C.46}$$

with,

$$\begin{aligned} \hat{\mathcal{H}}_F &= \hat{\mathcal{H}}_Z + \hat{\mathcal{H}}_Q \\ \hat{\mathcal{H}}_S &= \hat{\mathcal{H}}_\sigma + \hat{\mathcal{H}}_J + \hat{\mathcal{H}}_D \end{aligned} \tag{C.47}$$

whereas the fast ($\hat{\mathcal{H}}_\mathcal{F}$) and the slow Hamiltonian matrices ($\hat{\mathcal{H}}_\mathcal{S}$) are calculated separately.

After the construction of the fast Liouvillian $\hat{\hat{\mathcal{L}}}_{ZQ}$ with the fast Hamiltionian, the averaged slow Hamiltonian is calculated according to,

$$\overline{\hat{\mathcal{H}}}_S(t_i) = \lim_{\varepsilon \to 0} \frac{i\varepsilon}{i\varepsilon + \hat{\hat{\mathcal{L}}}_{ZQ}(t_i)} \hat{\mathcal{H}}_S(t_i) \tag{C.48}$$

Index i denotes that this procedure is done for all considered rotor phases/time steps respectively.

The time series of the averaged slow Hamiltonian is inverse Fourier transformed on an element by element basis, to get the coefficients $\overline{H_S}^{(j)}$ of

$$\overline{\hat{\mathcal{H}}}_S(t) = \sum_{j=-n}^{n} \overline{H_S}^{(j)} \, e^{i\, j\omega t} \tag{C.49}$$

In the next step the Floquet Liouvillian matrix is constructed with the Fourier components of the averaged slow Hamiltonian according to equation (C.31) and equation (C.38). This matrix is used in equation (C.43) to calculate the spectrum for one specific molecular orientation. The whole procedure is repeated for all considered orientations of the molecule and the single spectra are added to get the spectrum of a powdered sample.

Chapter D

Structure of *LanXSSQ*

1 Behaviour of the Fourier Components in the Transformed Averaged Slow Hamiltonian

The Hamiltonian in MAS experiments is time-dependent (see page 25). In Floquet theory we need to express this time-dependent Hamiltonian in the form of a Fourier series,

$$\hat{\mathcal{H}}(t) = \sum_{k=-\infty}^{\infty} H_k e^{i\,k\omega_R t} \tag{D.1}$$

with the time-independent Hamiltonian coefficients H_k. These coefficients can be calculated with inverse fast Fourier transformation of the calculated time series of the averaged slow Hamiltonian. The time-dependence of the Hamiltonian in MAS spectra of spin systems without quadrupolar coupling can be expressed in a 5 term Fourier series,[1] but in our case, the Hamiltonian was additionally projected (averaged) and therefore the resulting Fourier series is in principle infinite (eq. D.1).

The Fourier series coefficients are in general complex and the coefficients fulfill

[1] Simulations without quadrupolar coupling were done to check this property in LanXSSQ.

the relation,

$$H_n = (H_{-n})^* \tag{D.2}$$

because the Floquet matrix is Hermitian. In the presented diagrams (fig. D.1-D.3) the coefficients are presented in the form of their absolute values $|H_n|$. Also, only the positive coefficients are shown, because of the relation given in equation (D.2). Because of the Hermiticity of the Hamiltonian matrix,

$$\mathbb{H} = \left(\mathbb{H}^T\right)^* \tag{D.3}$$

only the elements H_{ij} with $i \leq j$ need to be considered; $H_{ij} = (H_{ji})^*$ for $i > j$. Note that the subscripts here denote matrix indices. The behaviour of the Fourier components of the Hamiltonian is studied here. In particular, we consider the decay of the Fourier components with index n. In addition, we investigate convergence of these numerically determined components with respect to number of rotor phase increments.

In principle the decaying behaviour changes with

- the Hamiltonian element,
- the orientation of the molecule in the MAS frame,
- the relative orientation of the tensors to each other,
- the relative strength of the quadrupolar interaction in comparison to the magnetic field interaction.

In Figure (D.1) Hamiltonian elements of the spin system ^{13}C-^{14}N in acetanilide are shown.[2] The straight lines in this figure show the exponential decay of the Fourier

[2]Note, the Hamiltonian elements in Diagrams (D.1-D.4) are plotted in a logarithmic scale. The input parameters are taken from Eichele *et al.* [23].

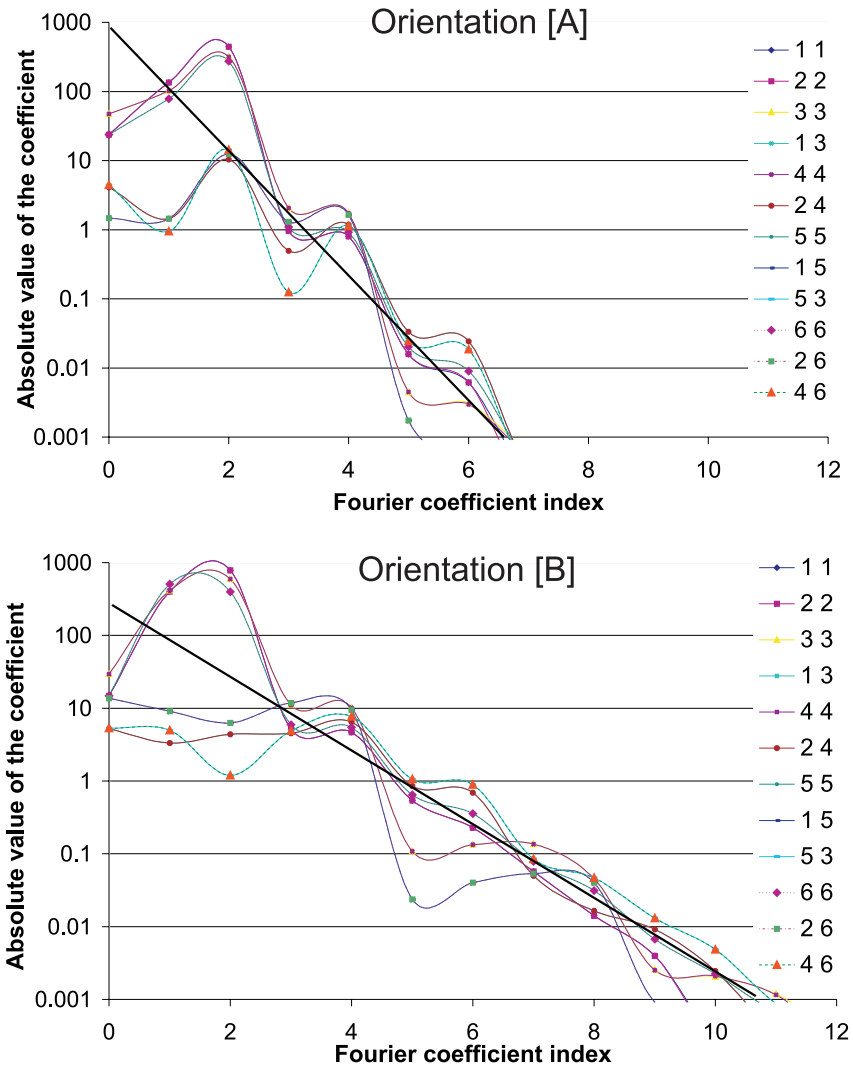

Figure D.1: Fourier coefficients of Hamiltonian elements of the spin system ^{13}C-^{14}N and their decaying properties for different orientations.

^{14}N quadrupolar coupling constant: 3.2 MHz, B_0=4.7 T

Orientation [A]: ϕ=285.0 $^\circ$, θ=112.5 $^\circ$

Orientation [B]: ϕ=22.5 $^\circ$, θ=3.2 $^\circ$

coefficients. The decaying behaviour is almost equivalent for all Hamiltonian matrix elements. However, it does depend on the molecular orientation (fig. D.1).

The decay rate of Hamiltonian matrix elements also depends on the relative orientation of the tensors. This is seen in the difference between graph [A] and graph [B] in figure D.2. On the other hand, the strength of the dipolar coupling doesn't influence the decaying behaviour(graph [B] and [C] in Figure D.2). The absolute values of the coefficients change, but the slope of the straight line remains the same in both graphs. This also applies to the chemical shielding.

In Figure (D.3) the calculated Fourier components of some Hamiltonian elements for the ^{13}C-^{35}Cl spin pair at three different magnetic fields are shown. The input parameters were taken from Eichele *et al.* [18]. The general decaying trend is again indicated with a straight line. At a high magnetic field (relatively weak quadrupole interaction) the coefficients decay quickly, but in case of dominant quadrupolar interaction at a field strength of 2.4T the decay is quite slow. In general it can be pointed out that an increasing quadrupolar coupling interaction or decreasing magnetic field strength necessitates the use of more Fourier components - chosen according to a specific truncation threshold.

In the next step the dependence of the Fourier coefficients on the number of γ_R increments is considered. In Figure (D.4) the absolute values of the Fourier coefficients of one Hamiltonian matrix element is presented. The difference of these coefficients is about 10^{-2} and does not depend on their absolute value. Therefore the relative error between the coefficients with large values (> 0.1) is distinct below 1%, but the small valued coefficients (<0.01) are almost arbitrary, if they are calculated with a small number of increments. This behaviour is, as far as investigated, independent of Hamiltonian elements, orientation of the molecule and the spin system. The variation of γ_R increments in the range from 256 to 8192 have no effect in the calculated spectrum. It is even possible to cut off all Fourier coefficients which

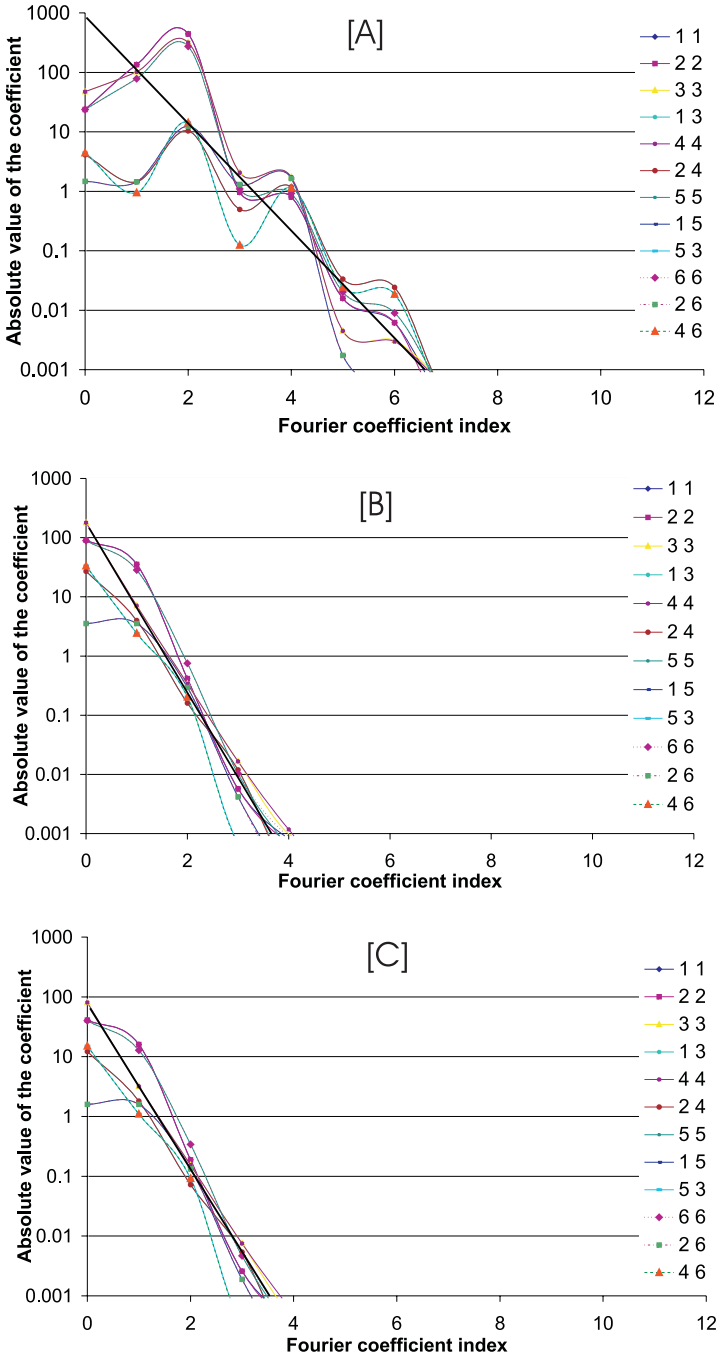

Figure D.2: Fourier coefficients of Hamiltonian elements of the spin system ^{13}C-^{14}N and their decaying properties for a different relative tensor orientation and dipolar coupling.

Quadr. coupling constant: 3.2 MHz Orientation: ϕ=22.5 $^\circ$, θ=3.2 $^\circ$ B_0=4.7 T

[A]: equals A in Figure (D.1)

[B]: all tensors are lined up

[C]: like b, but with reduced dipolar coupling (390 Hz instead of 865 Hz)

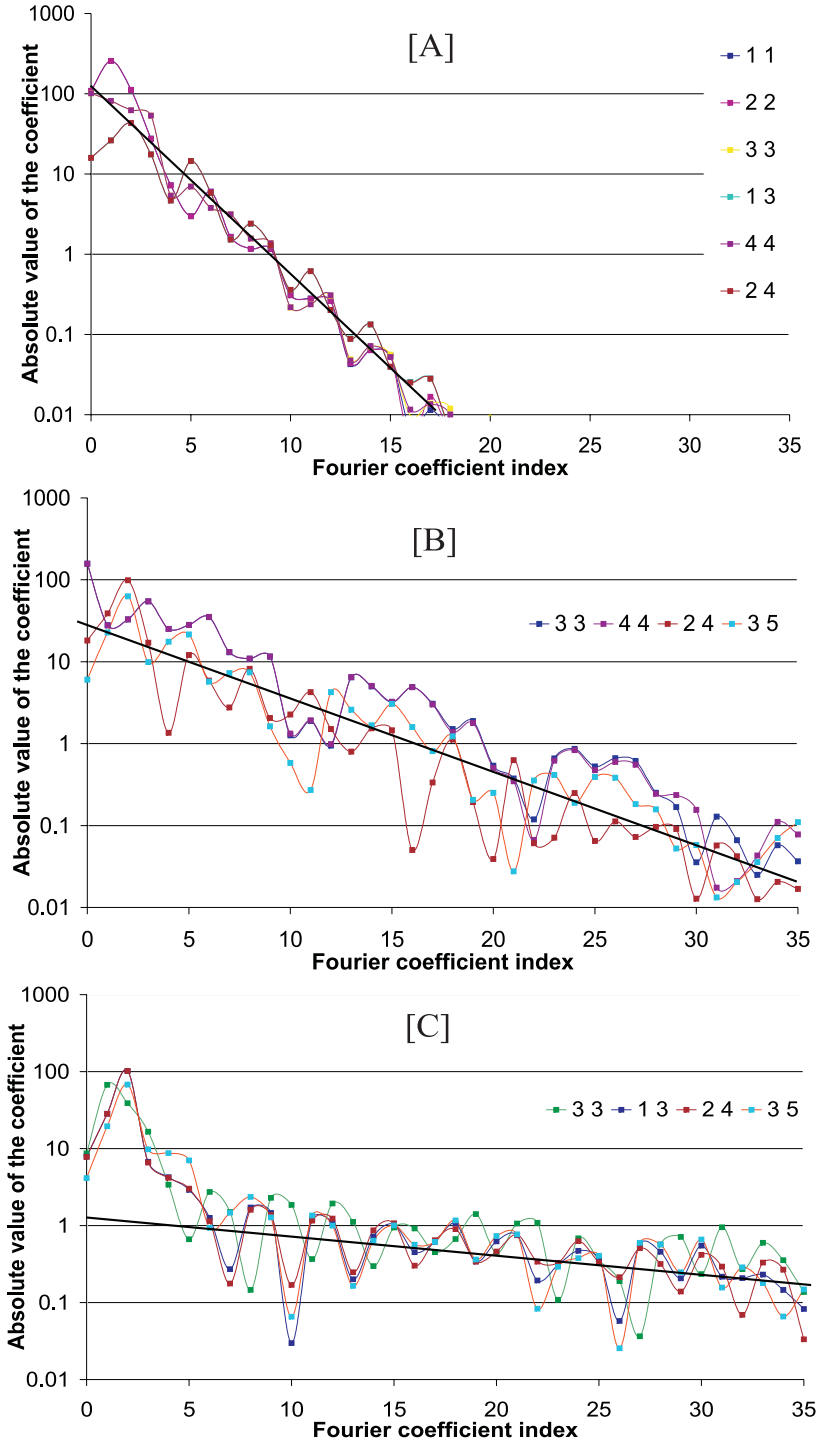

Figure D.3: Fourier coefficients of Hamiltonian elements of the spin system ^{13}C-^{35}Cl and their decaying properties for different magnetic fields.

^{35}Cl quadrupolar coupling constant: 72 MHz Orientation: ϕ=45.0 $^\circ$, θ=53.1 $^\circ$

[A]: 9.4 T, [B]: 4.7 T, [C]: 2.4 T

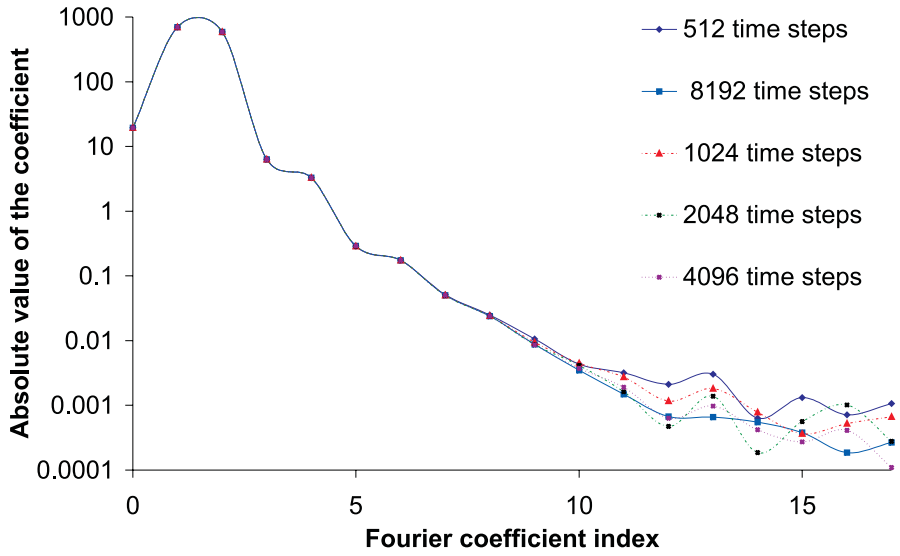

Figure D.4: Fourier coefficients of a Hamiltonian element calculated with different numbers of γ_R increments/time steps.

are lower than 0.2 without any effects in the simulated spectrum. If the truncation is done for a lower threshold (e.g. 10^{-6}), than the Lanzcos method [22] can have convergence problems when not enough γ_R increments were used.

The results presented here demonstrate that the Fourier series of the Hamiltonian decays exponentially, but the rate of decay varies. Mainly it dependents on the strength of the quadrupole interaction in comparison to the magnetic interaction. The dependence on molecular orientation and tensor arrangement on the other side is not as distinct.

The number of coefficients which should be used to convert the simulated spectrum depends on many parameters. In the Floquet matrix the Fourier coefficients with higher indices get less important, which is a result of the convergence criteria of the Floquet expansion. Therefore it is possible, that even large coefficients can be omitted without a change in the spectrum. In principle, when there are

many spinning sidebands in a simulated spectrum more Floquet blocks and hence Fourier components will be required for convergence. However, truncation of all small components (smaller than 1% of the largest coefficient values) is, as far as investigated, invisible in simulated spectra. It is also recommended that relatively few γ_R increments be used to speed up the calculation.

2 Dependence of Resonance Frequencies on Molecular Orientation

The resonance frequencies of the spin half nucleus depend on the absolute orientation of the molecule in the MAS reference frame. In case of small quadrupolar coupling, the frequencies for the fast spinning limit can be calculated with perturbation theory expressions [5], which is shown in graph [A] of figure (D.5). The dotted lines show the calculated frequencies with *LanXSSQ*. In both cases equivalent input parameters were used. The trend of the lower frequency is almost equivalent for perturbation theory and our program. But the orientation dependence of the higher frequency is quite different. In particular, whereas perturbation theory predicts degeneracy of the two higher frequencies, *LanXSSQ* produces two distinct frequencies for most orientations. However, the former prediction is more in keeping with experimental observations (F.3). The trouble with *LanXSSQ* is that it ignores the effects of T_2 relaxation - in particular, the T_2 relaxation of the quadrupolar nucleus.

In case of fast T_2 relaxation of the quadrupolar nucleus (i.e. fast compared with sample spinning), the quadrupolar nucleus is always in a mixture of $\hat{\mathcal{H}}_F$ eigenstates even though such states vary with sample spinning. The rapid T_2 relaxation quenches coherences resulting from the changing of $\hat{\mathcal{H}}_F$ eigenstates.

In the perturbation approach, the frequency calculation is done in the quadrupole eigenbasis, with the quadrupolar nucleus taken to be in a mixture of eigenstates.

This corresponds to Fourier analyzing resonance frequencies with respect to rotor phase instead of Fourier analyzing the Hamiltonian, as prescribed by average Hamiltonian theory.

In case of large quadrupolar coupling, inverse perturbation theory is used to calculate the orientation dependent resonance frequencies of the spin-$\frac{1}{2}$ nucleus coupled to a spin-$\frac{3}{2}$ quadrupolar nucleus (solid lines in graph [B] of fig. D.5). The with *LanXSSQ* calculated frequencies are again quite different (dotted lines in graph [B] of fig. D.5) for the same reason as in the case of weak quadrupolar interaction. Again, experimental observations are more in accord with the inverse perturbation theory with fast T_2 relaxation [18].

For both cases, weak and strong quadrupolar interaction, the basis of our simulation program was changed to the quadrupole eigenbasis to calculate the resonance frequencies for the fast relaxation limit of the quadrupolar nucleus. The resultant frequencies are shown in graph [A] and [B] respectively of figure D.5 (green triangles). *LanXSSQ* produces almost equivalent orientation dependent resonance frequencies compared to the perturbation approaches. However, computed spectra, shown in Figure (F.3), show that the fast quadrupolar T_2 relaxation assumption may not be exactly correct, because the relative intensities of the simulated bands do not match the experimental spectrum. Future work will focus on implementation of finitely fast quadrupolar T_2 relaxation. The *LanXSSQ* program is well suited to such implementation.

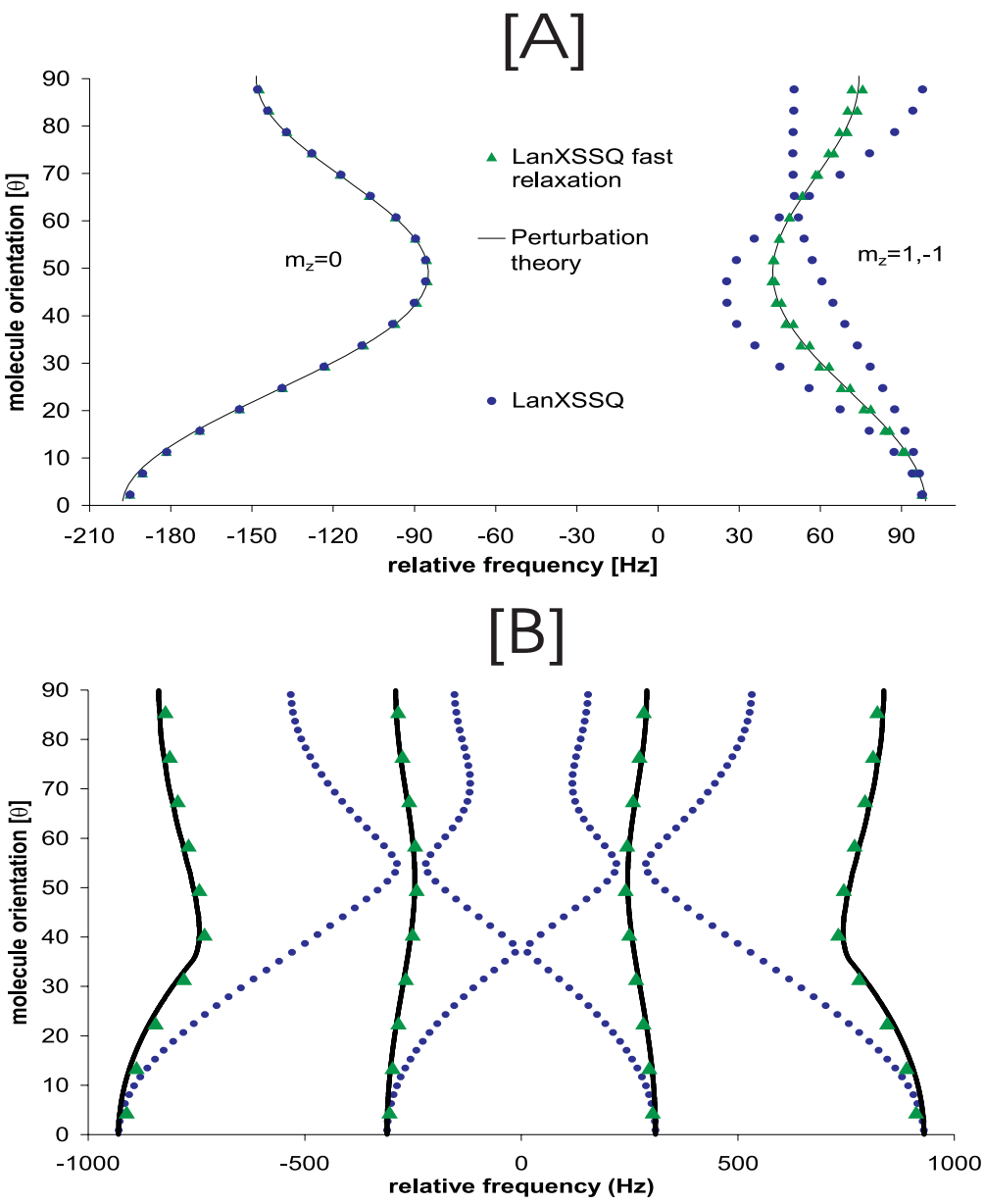

Figure D.5: Molecular orientation dependence of the resonance frequencies. A Comparison between *LanXSSQ* and perturbation theory.

All tensors (dipolar and quadrupolar) in these simulations have the same direction and they are axially symmetric. The angle between the z-axes of the MAS frame and the cylindrical symmetric spin system is given by Θ.

[A]: Spin-1 coupled to spin-$\frac{1}{2}$, with weak quadrupole interaction

[B]: Spin-$\frac{3}{2}$ coupled to spin-$\frac{1}{2}$, approximately infinite quadrupolar interacion

Chapter E

Experimental

1 Synthesis of ^{13}C-Labeled Acetanilide

An interesting well researched system with residual $^{13}C - ^{14}N$ dipolar coupling is acetanilide [23]. To simplify the ^{13}C solid state NMR-spectra and increase the signal to noise, the syntheses of ^{13}C-enriched acetanilide (**I**) was necessary (fig. E.1).

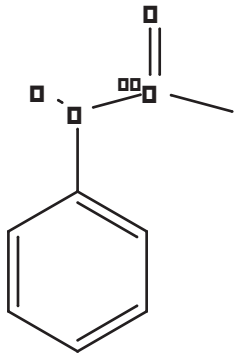

Figure E.1: Structure of ^{13}C-labeled acetanilide

Compound (**I**) is synthesized according to following reaction,

$$NaCH_3CO_2 + C_6H_5NH_2 \xrightarrow{1d,\ EDC\cdot HCl} (C_6H_5)NH(COCH_3) + \text{"NaOH"}$$

EDC = 1 − [3 − Dimethylaminopropyl] − 3 − ethylcarbodiimide

and it was prepared by dissolving 0.62 g of ^{13}C-sodium acetate (7.5 mmol) and 1.52 g EDC (10.0 mmol) in 25 ml dried tetrahydrofuran. To the stirred mixture 0.68 ml fresh distilled aniline (7.5 mmol) was added. Then the suspension was stirred for one day. After evaporation of the solvent, 50 ml water with 1 ml conc. HCl was added. The crystallized product was separated and vacuum dried. ^{1}H-NMR (fig. E.2) and a ^{13}C-NMR spectrum (fig. E.3) were obtained on a Bruker AC-200 in deuterated chloroform as solvent to specify the purity.

The proton and carbon spectra show the J-coupling between the labeled carbonyl group and the neighboring hydrogen and carbon atom respectively. Also almost no signals from the starting materials are present and the product is used without further purifications.

Figure E.2: ^{1}H-NMR spectrum (200.13 MHz) of ^{13}C-acetanilide recorded in chloroform solvent at room temperature

Figure E.3: ^{13}C-NMR spectrum (50.32 MHz) of ^{13}C-acetanilide recorded in chloroform solvent at room temperature

2 X-ray Crystal Structure Determination of Acetanilide

The crystal was centered on a P4 Siemens diffractometer, equipped with a Siemens SMART 1K charge-coupled device (CCD) area detector (using the program SMART) and a rotating anode using graphite-monochromated Mo-$K\alpha$ radiation ($\lambda = 0.71073$ nm). The diffraction data collection consisted of a full Ψ rotation at $\chi = 0°$ using $0.3°$ frames, followed by a series of short (100 frames) ω scans at various Ψ and χ settings to fill the gaps. The crystal-to-detector distance was $5.000cm$, and the data collection was carried out in a 512×512 pixel mode using 2×2 pixel binning. Processing was carried out by using the program SAINT, which applied Lorentz and polarization corrections to three-dimensionally integrated diffraction spots. The program SADABS was used for the scaling of diffraction data, the application of a decay correction, and an empirical absorption correction based on redundant reflections.

The XPREP program was used to confirm the unit cell dimensions and the crystal lattice. The final refinement of the structure was obtained by introducing anisotropic parameters for all the atoms, except the hydrogen atoms, an extinction parameter, and the recommended weight factor.

The calculations were performed with the SHELXL package for structure determination, refinement, and molecular graphics.

The data collection parameters and crystallographic information are summarized in table (E.1). The bond length, bond angles and dihedral angles are listed in table (E.2). The results are in good agreement to previous obtained x-ray and low temperature neutron diffraction data [24, 25]. In figure (E.4) the geometry of one acetanilide molecule in the crystal is shown. Interesting is the fact that the molecule is not planar (fig. E.5) (torsion angle C(7)-N(1)-C(1)-C(2)=19.4 $^\circ$), which has effects in the strength of the electric field gradient, chemical shielding anisotropy and orientation of the considered tensors in the C-N spin system. It exists a strong hydrogen bonding between acetanilide molecules in the crystal (fig. E.6).

Table E.1: Summary of Crystal Data and Refinement Results for acetanilide

empirical formula	C_8H_9NO
space group (No.)	*Pbca*(61)
a (Å)	9.498(6)
b (Å)	8.002(6)
c (Å)	19.656(14)
α (°)	90
β (°)	90
γ (°)	90
V (Å^3)	1493.8(18)
$\frac{\text{molecules}}{\text{unit cell}}$	8
M $\left(\frac{g}{mol}\right)$	135.16
calculated density $\left(\frac{g}{cm^3}\right)$	1.202
T (K)	298(2)
μ $\left(\frac{1}{mm}\right)$	0.080
λ (Å) used for data collection	0.71073
final agreement factors	R_1=0.0427
	wR_2=0.0918

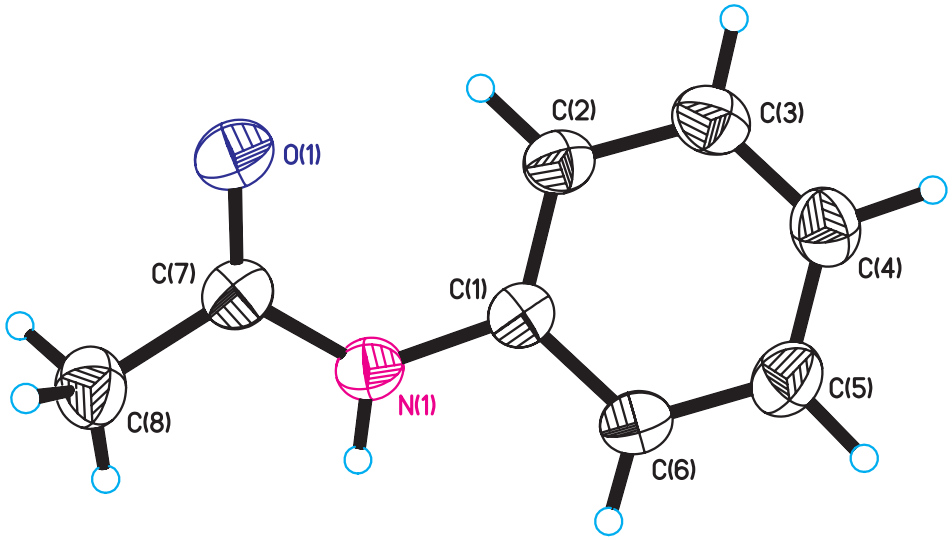

Figure E.4: Structure of acetanilide (X-ray data)

The distance between the hydrogen atom and the oxygen is 193.4 pm. Figure (E.7) and (E.8) show the packing of the crystal. Two different kind of layers can be distinguished, first the hydrogen bonding layer (hydrophilic) and second the layer with the stacked aromatic rings (hydrophobic). The packing of the molecule and especially the energy gain of the hydrogen bond compensates the energetic disadvantage of the twisting.

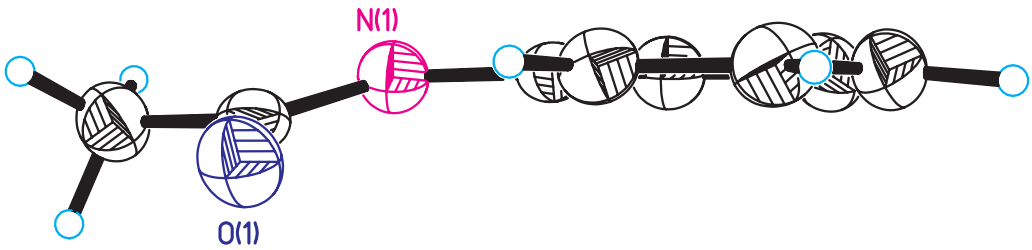

Figure E.5: Twisted geometry of acetanilide (X-ray data)

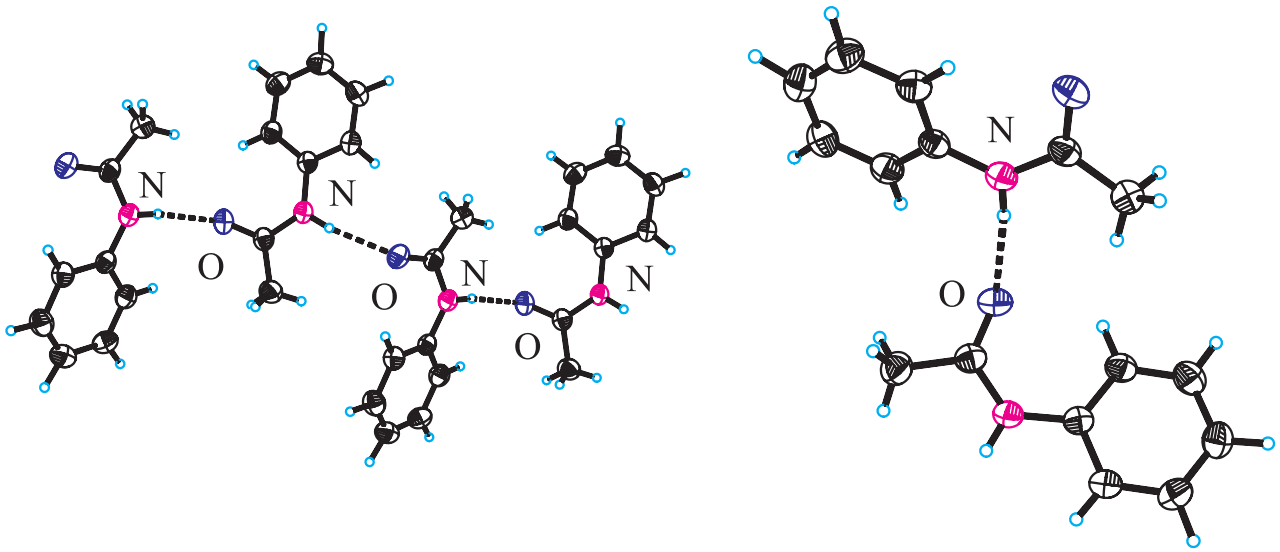

Figure E.6: Hydrogen bonding between acetanilide molecules in the crystal

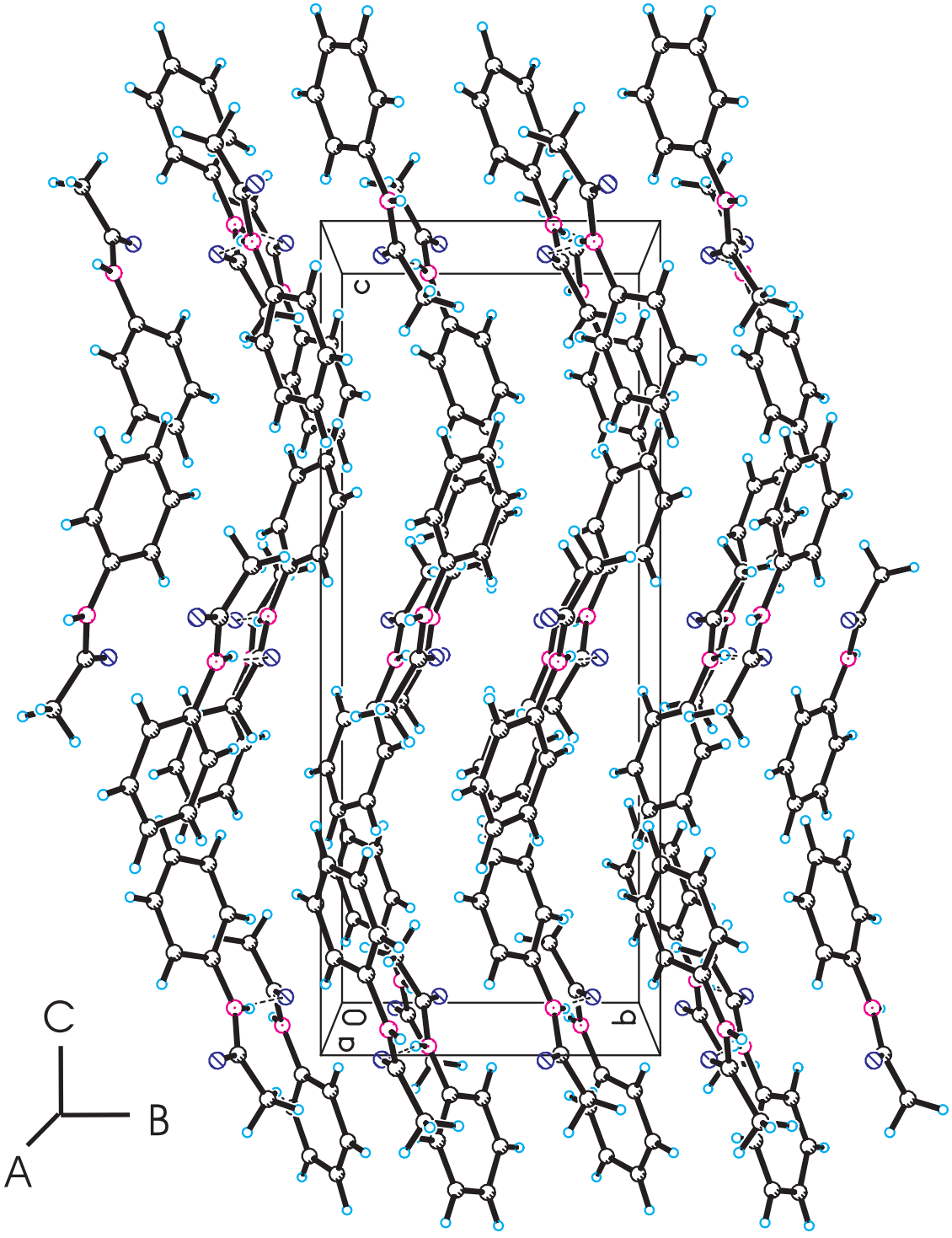

Figure E.7: Packing of acetanilide in the orthorhombic crystal (view 1)

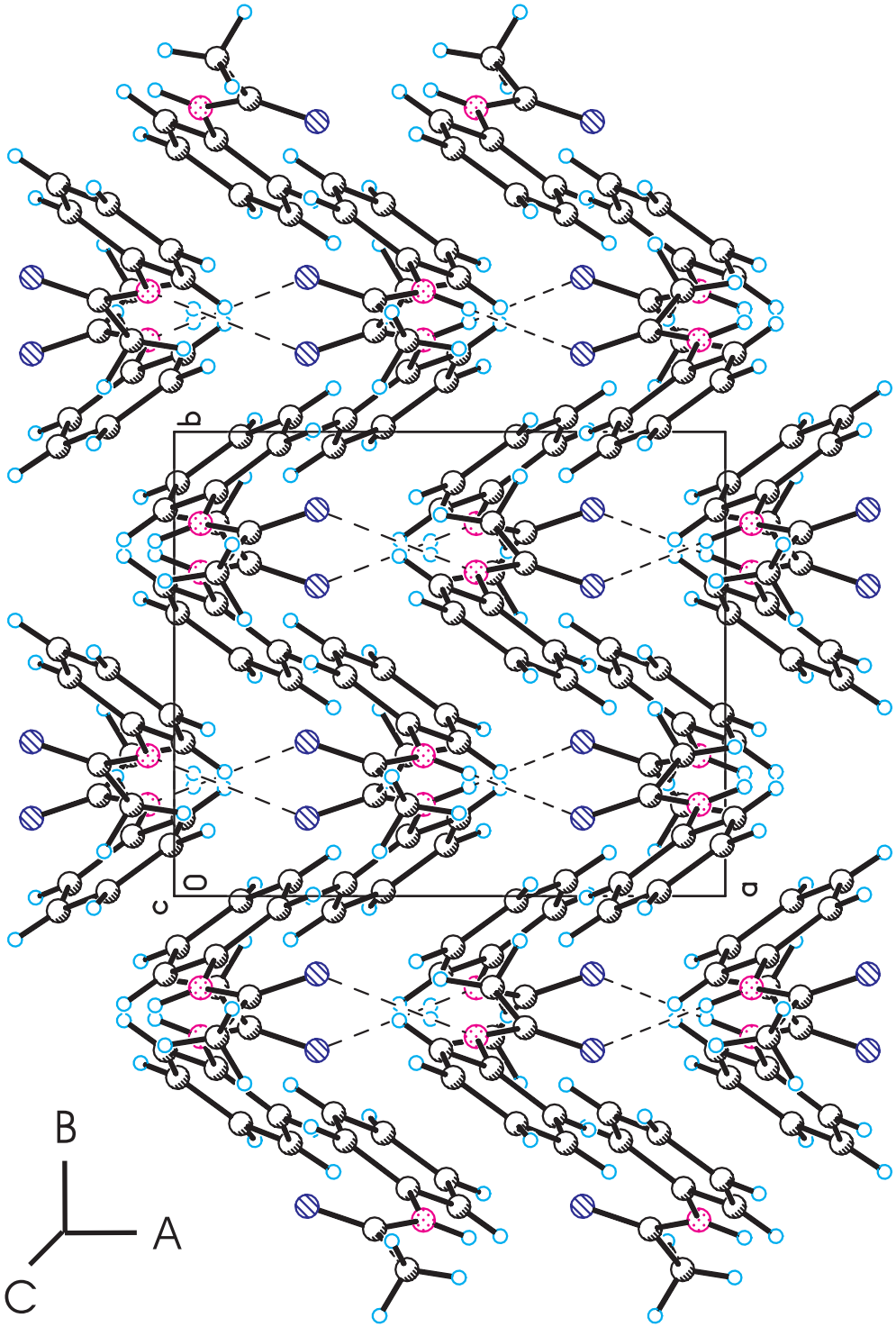

Figure E.8: Packing of acetanilide in the orthorhombic crystal (view 2)

Table E.2: Bond lengths, bond angles and torsion angles for acetanilide

Atoms	Bond length [pm]	Atoms	Bond angles [°]	Atoms	Torsion angles [°]
O(1)-C(7)	122.8(3)	C(6)-C(1)-C(2)	119.1(3)	C(7)-N(1)-C(1)-C(2)	-19.4(4)
N(1)-C(7)	134.8(3)	C(6)-C(1)-N(1)	117.5(3)	C(7)-N(1)-C(1)-C(6)	160.5(3)
N(1)-C(1)	141.0(3)	C(2)-C(1)-N(1)	123.4(2)	C(6)-C(1)-C(2)-C(3)	-1.2(4)
C(1)-C(6)	138.3(4)	C(3)-C(2)-C(1)	119.3(3)	N(1)-C(1)-C(2)-C(3)	178.7(2)
C(1)-C(2)	138.6(3)	C(4)-C(3)-C(2)	121.4(3)	C(1)-C(2)-C(3)-C(4)	-0.3(4)
C(2)-C(3)	138.5(4)	C(3)-C(4)-C(5)	119.0(3)	C(2)-C(3)-C(4)-C(5)	1.4(4)
C(3)-C(4)	137.3(4)	C(6)-C(5)-C(4)	120.4(3)	C(3)-C(4)-C(5)-C(6)	-1.0(4)
C(4)-C(5)	137.6(4)	C(5)-C(6)-C(1)	120.8(3)	C(4)-C(5)-C(6)-C(1)	-0.4(4)
C(5)-C(6)	137.6(4)	O(1)-C(7)-N(1)	122.6(3)	C(2)-C(1)-C(6)-C(5)	1.5(4)
C(7)-C(8)	149.4(4)	O(1)-C(7)-C(8)	121.3(3)	N(1)-C(1)-C(6)-C(5)	-178.4(2)
		N(1)-C(7)-C(8)	116.1(3)	C(1)-N(1)-C(7)-O(1)	3.2(4)
				C(1)-N(1)-C(7)-C(8)	-176.2(3)

3 Solid State NMR Spectra of Acetanilide

The ^{13}C solid state CP/MAS spectra were obtained at 50.323 MHz on a Bruker DSX-200 (B_0=4.7 T) and at 100.630 MHz on a Bruker DSX-400 (B_0=9.4 T) spectrometer. Crystalline samples were ground packed into 4 mm zirconium oxide rotors. All spectra are obtained at room temperature. Cross-polarization (CP) was achieved under Hartmann-Hahn matching condition using 90 $^\circ$ pulses of 3.0 μs. The optimum contact time was found to be approximately 4 ms. The spectra were acquired with high-power ^1H decoupling. A recycle time of 20 s was used to acquire the ^{13}C spectra.

Figure (E.9) shows the static powder pattern from ^{13}C labeled acetanilide at a magnetic field strength of 4.7 T. The other spectra are maintained at different rotation speeds around the magic angle. The spinning speed were varied from 200 Hz to 8kHz. The spectra are maintained at 4.7 T (fig. E.10-E.16)and at 9.4 T (fig. E.17-E.21) respectively.

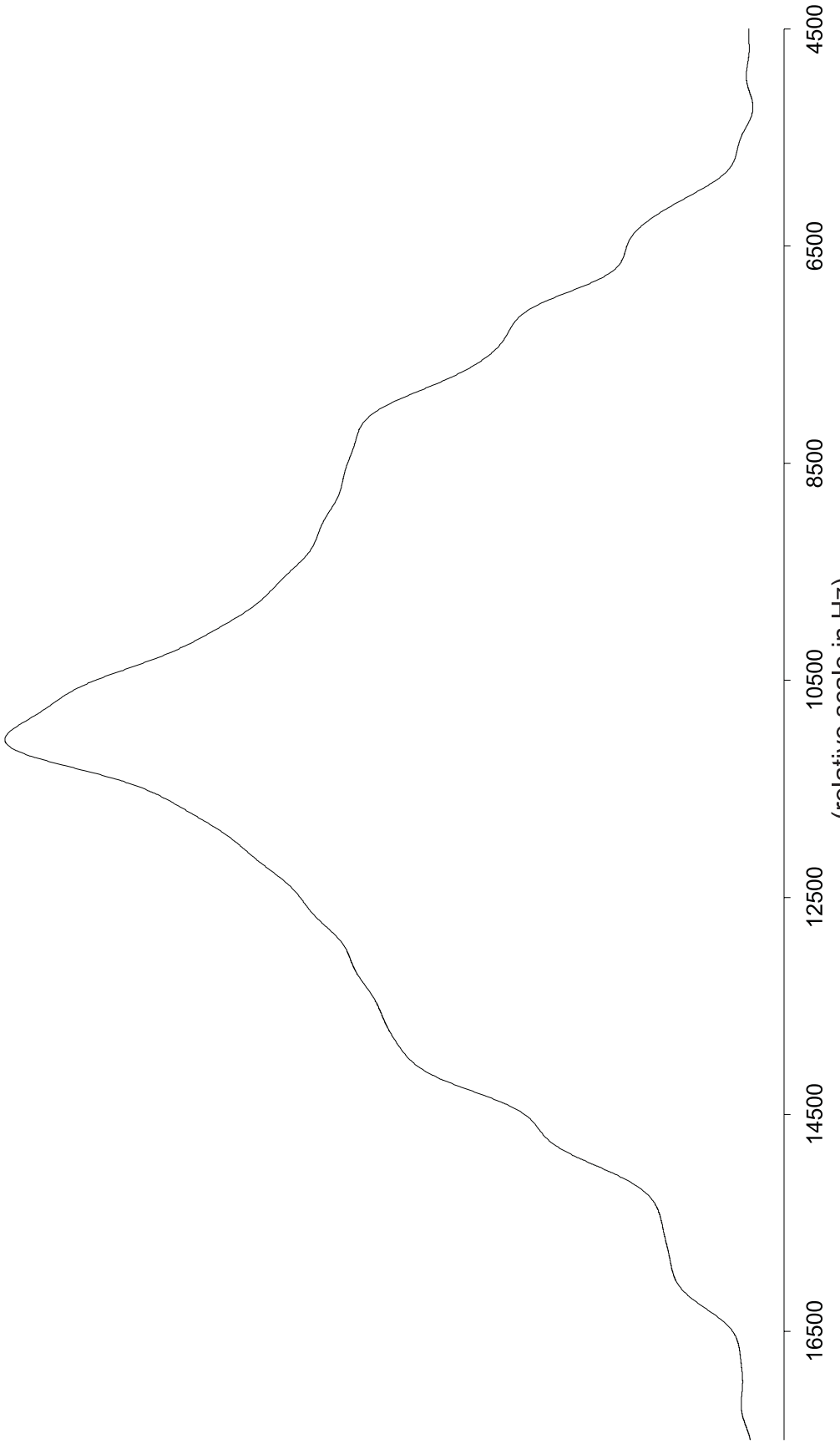

Figure E.9: Static CP/MAS ^{13}C-NMR spectrum (50.32 MHz) of ^{13}C-acetanilide

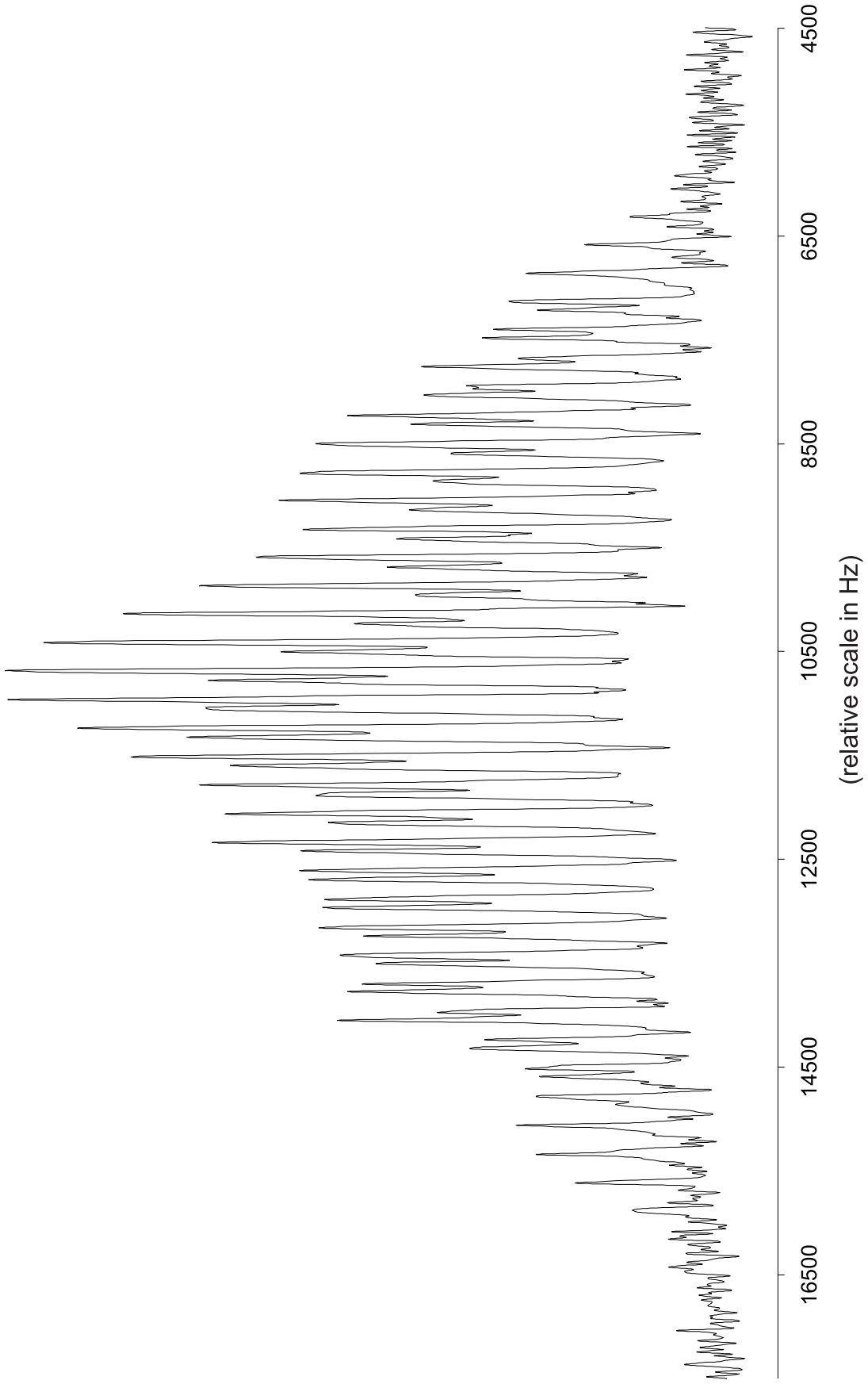

Figure E.10: CP/MAS ^{13}C-NMR spectrum (50.32 MHz) of ^{13}C-acetanilide at a spinning rate of 274 Hz±2 Hz

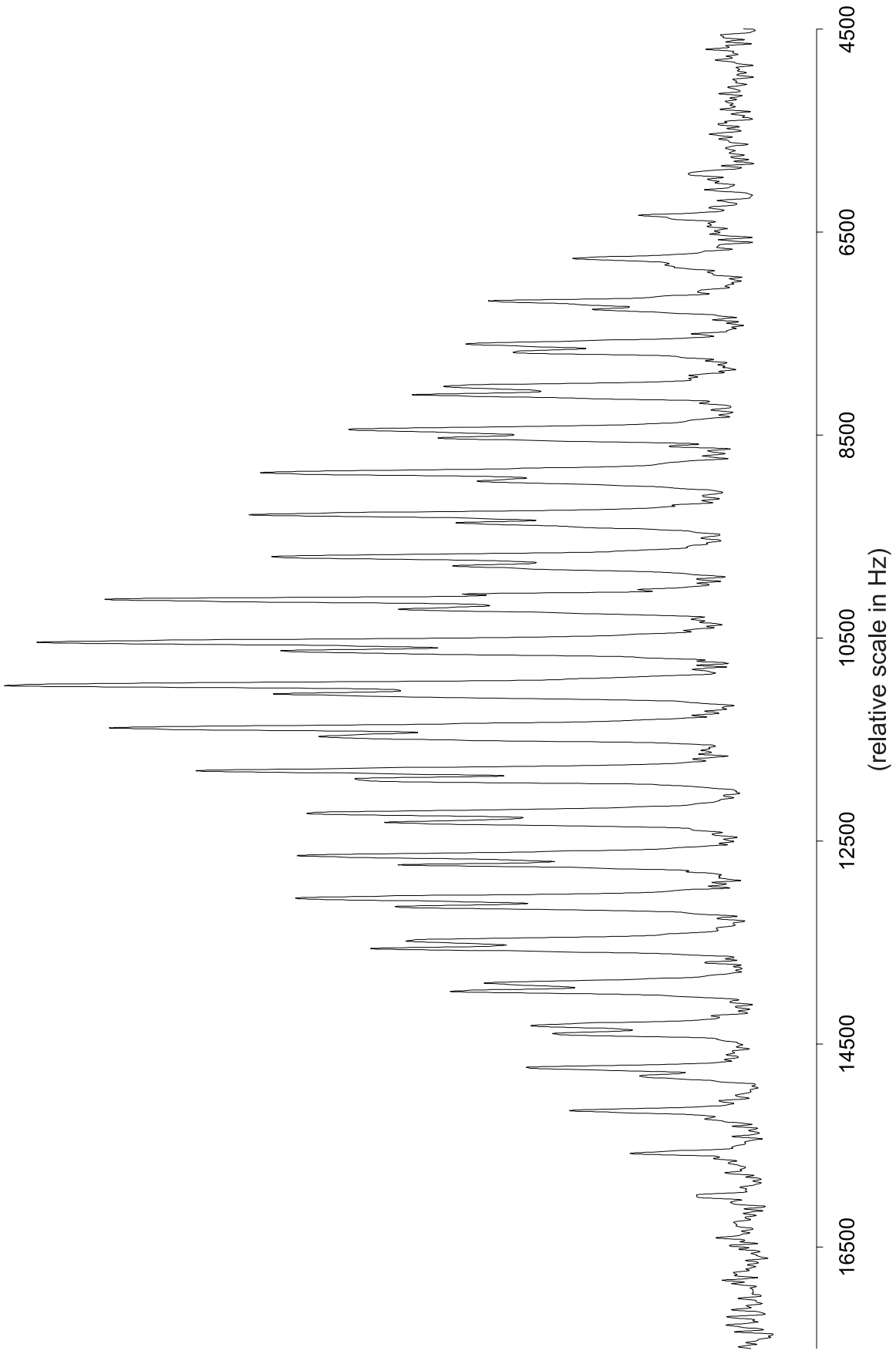

Figure E.11: CP/MAS ^{13}C-NMR spectrum (50.32 MHz) of ^{13}C-acetanilide at a spinning rate of 417 Hz±2 Hz

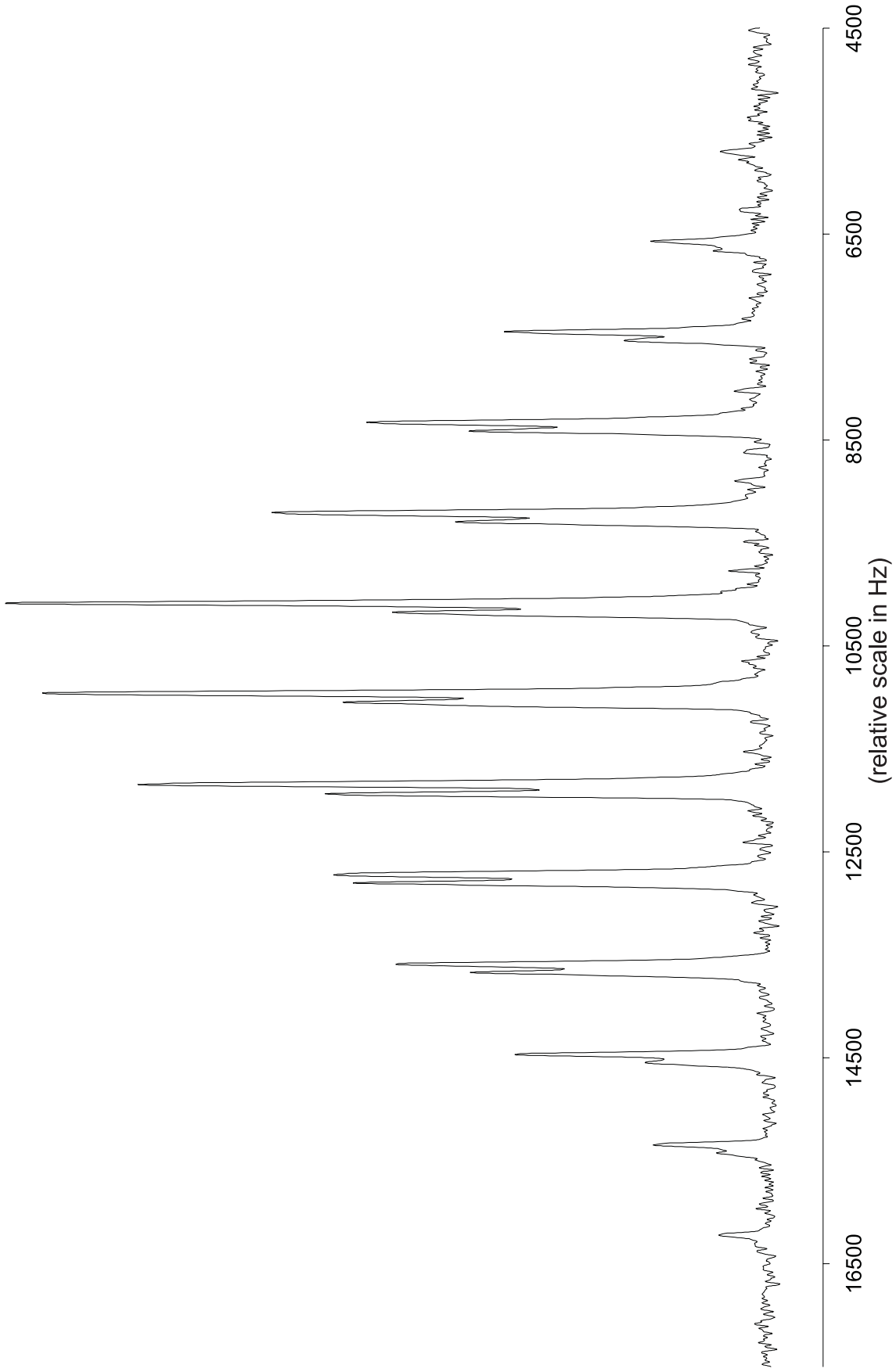

Figure E.12: CP/MAS ^{13}C-NMR spectrum (50.32 MHz) of ^{13}C-acetanilide at a spinning rate of 875 Hz±1 Hz

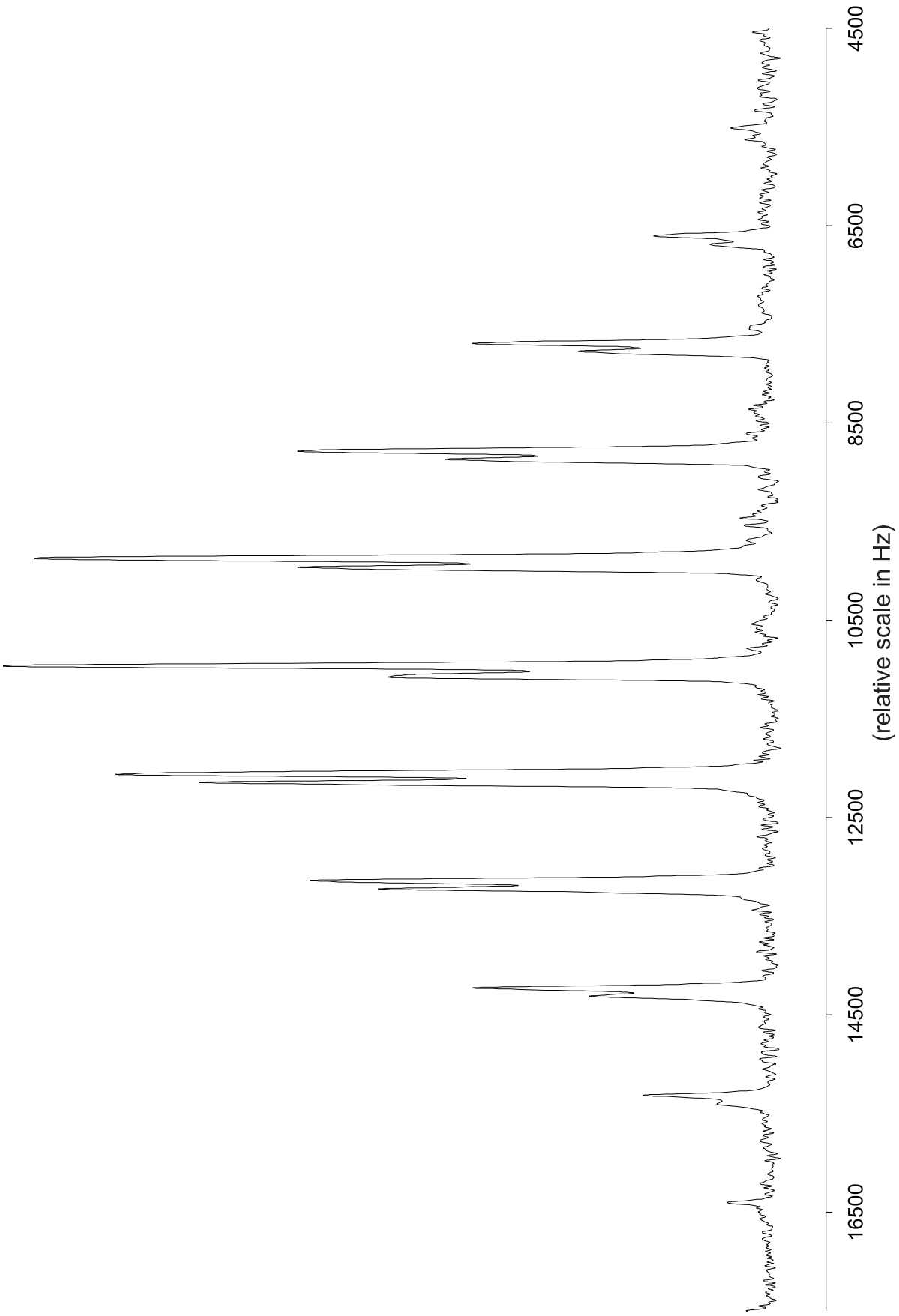

Figure E.13: CP/MAS ^{13}C-NMR spectrum (50.32 MHz) of ^{13}C-acetanilide at a spinning rate of 1088 Hz±2 Hz

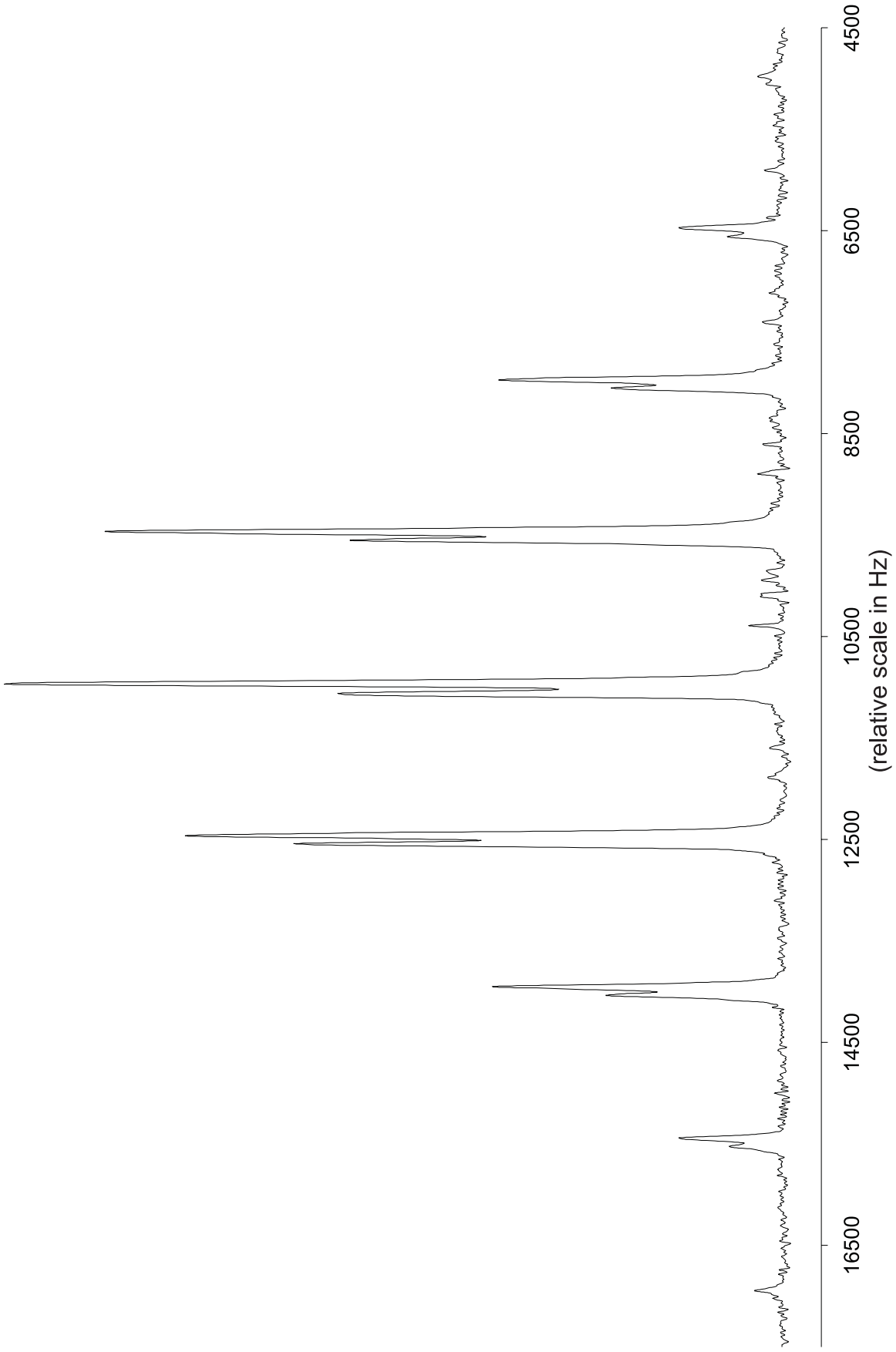

Figure E.14: CP/MAS ^{13}C-NMR spectrum (50.32 MHz) of ^{13}C-acetanilide at a spinning rate of 1495 Hz±2 Hz

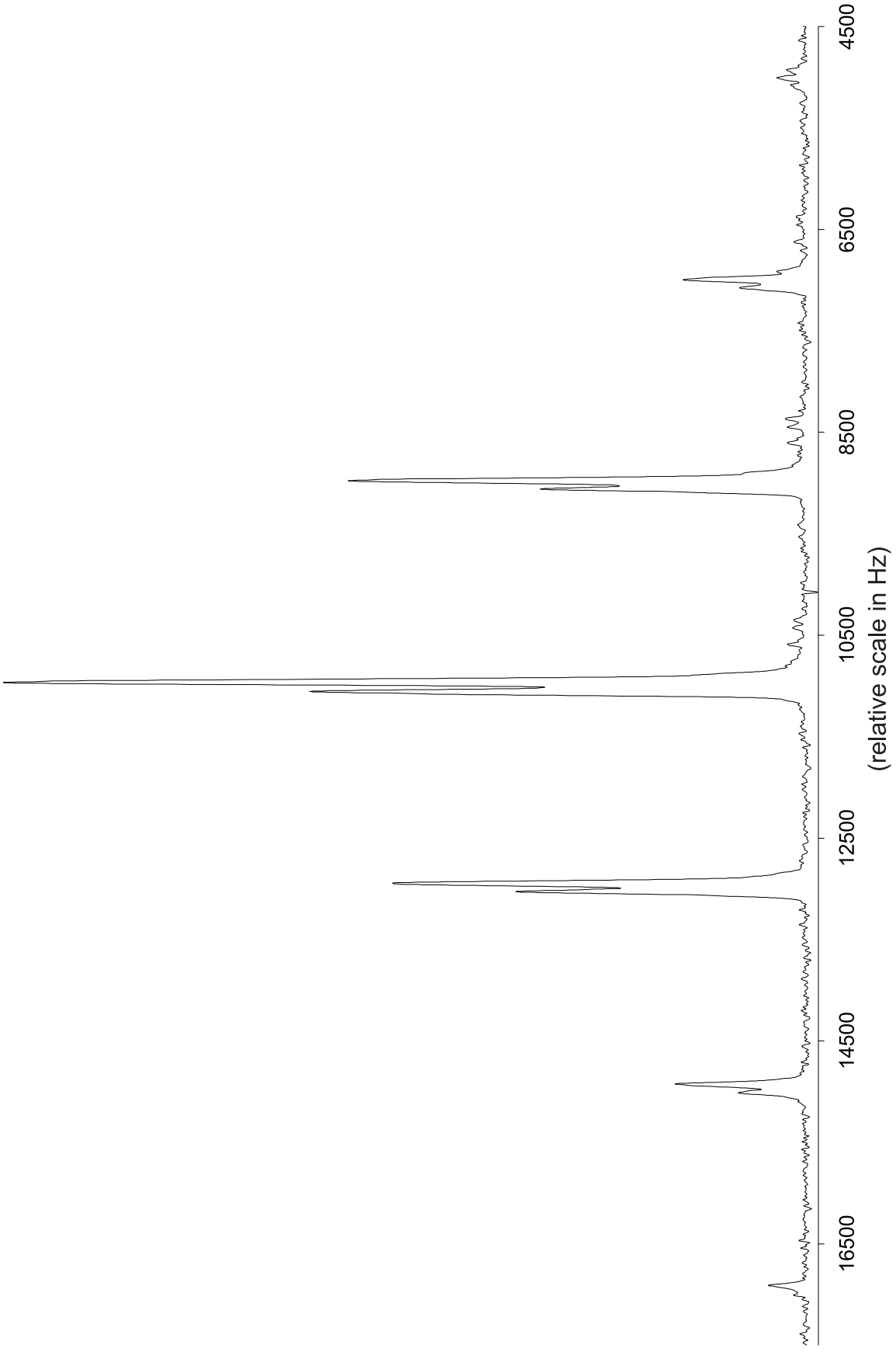

Figure E.15: CP/MAS ^{13}C-NMR spectrum (50.32 MHz) of ^{13}C-acetanilide at a spinning rate of 1991 Hz±1 Hz

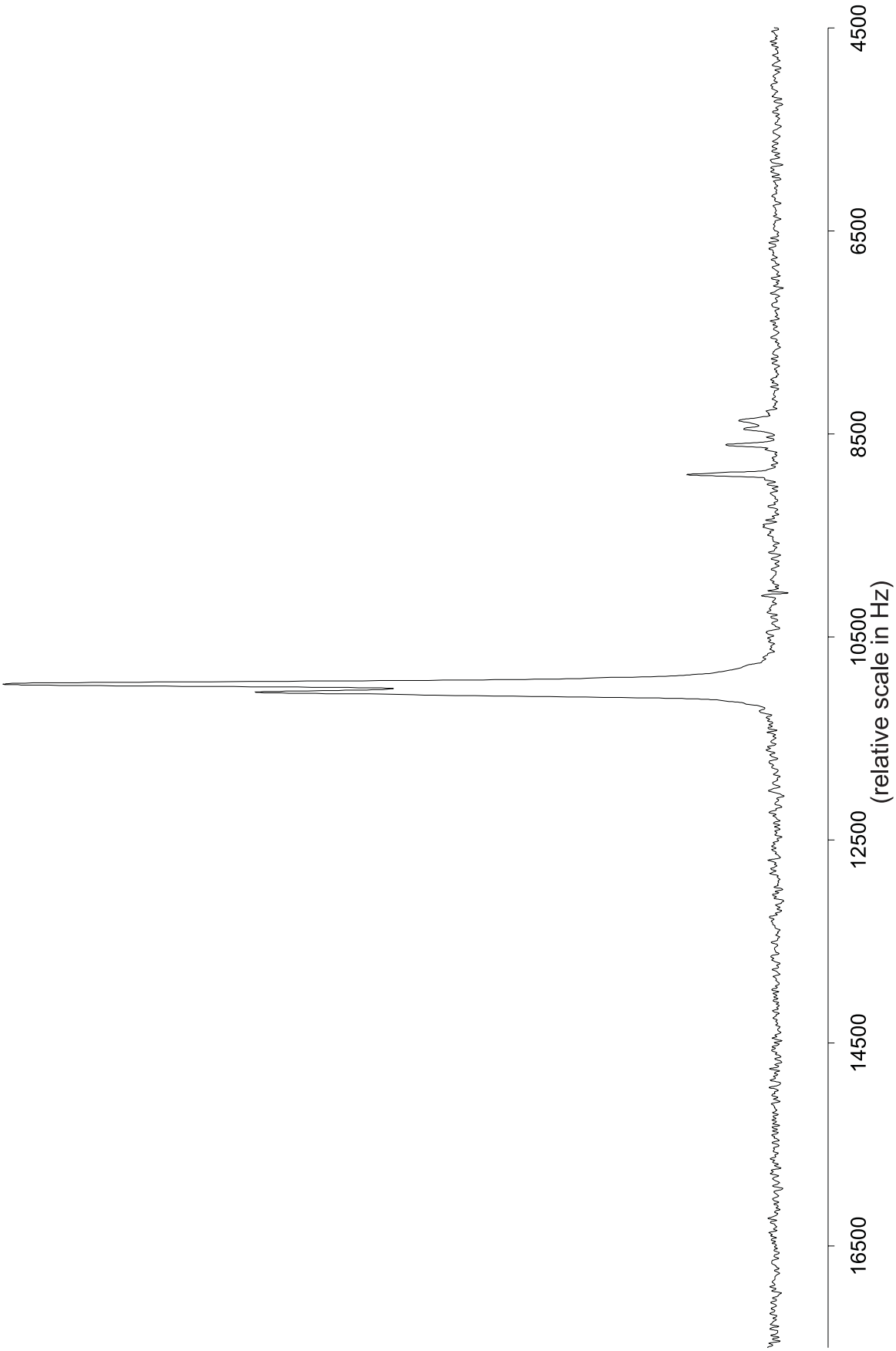

Figure E.16: CP/MAS ^{13}C-NMR spectrum (50.32 MHz) of ^{13}C-acetanilide at a spinning rate of 8054 Hz±2 Hz

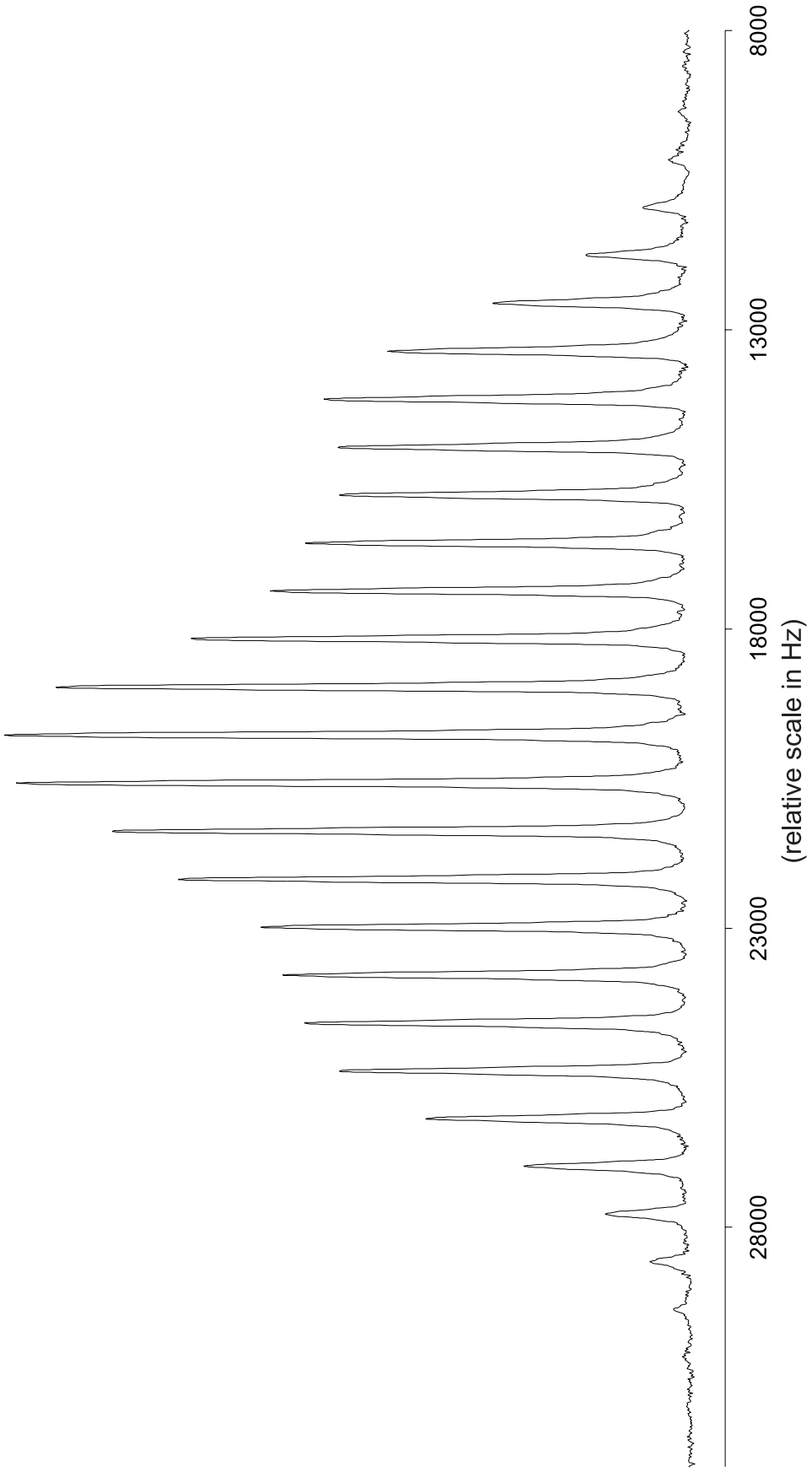

Figure E.17: CP/MAS ^{13}C-NMR spectrum (100.6 MHz) of ^{13}C-acetanilide at a spinning rate of 800 Hz±2 Hz

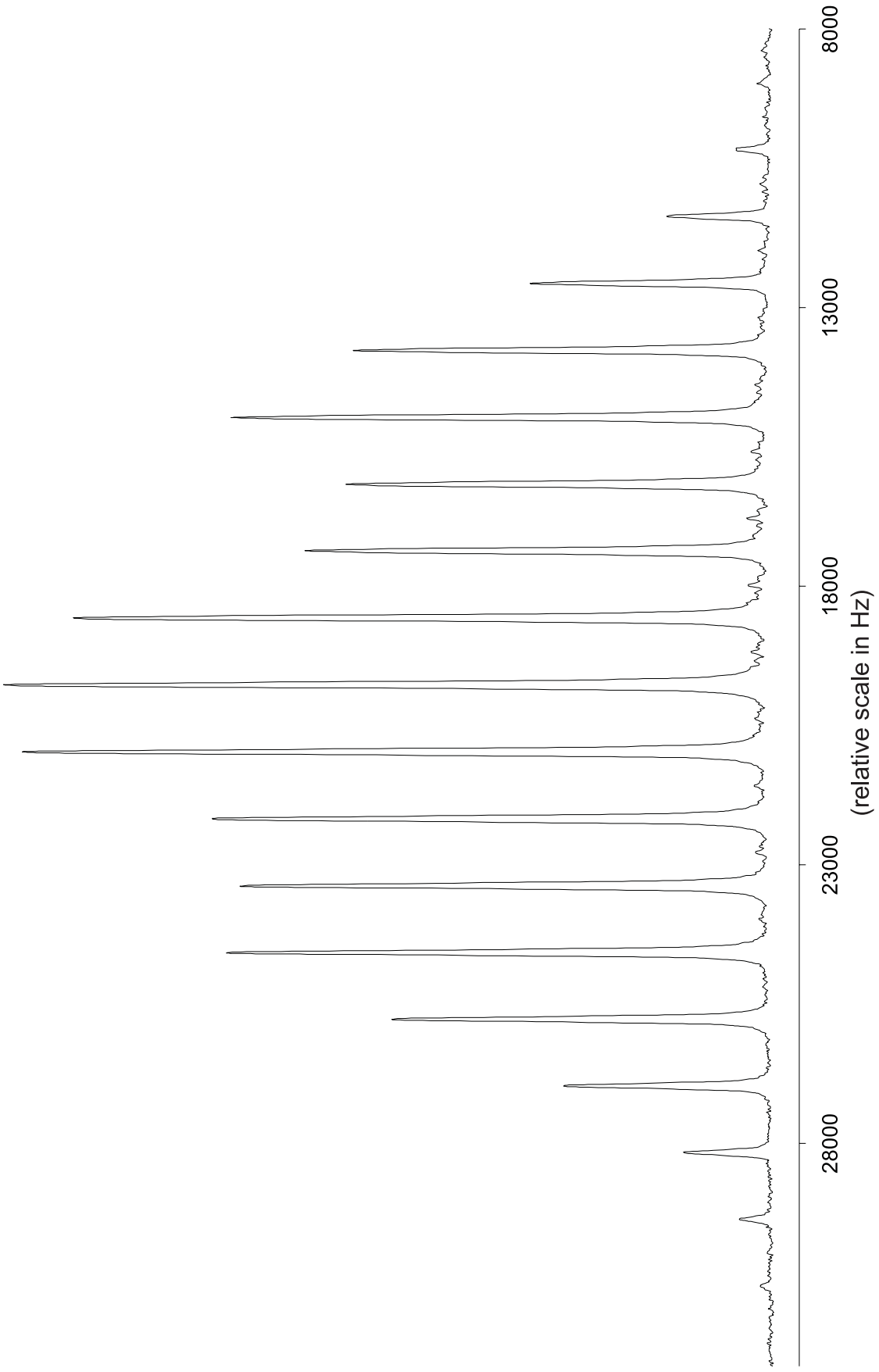

Figure E.18: CP/MAS ^{13}C-NMR spectrum (100.6 MHz) of ^{13}C-acetanilide at a spinning rate of 1200 Hz±2 Hz

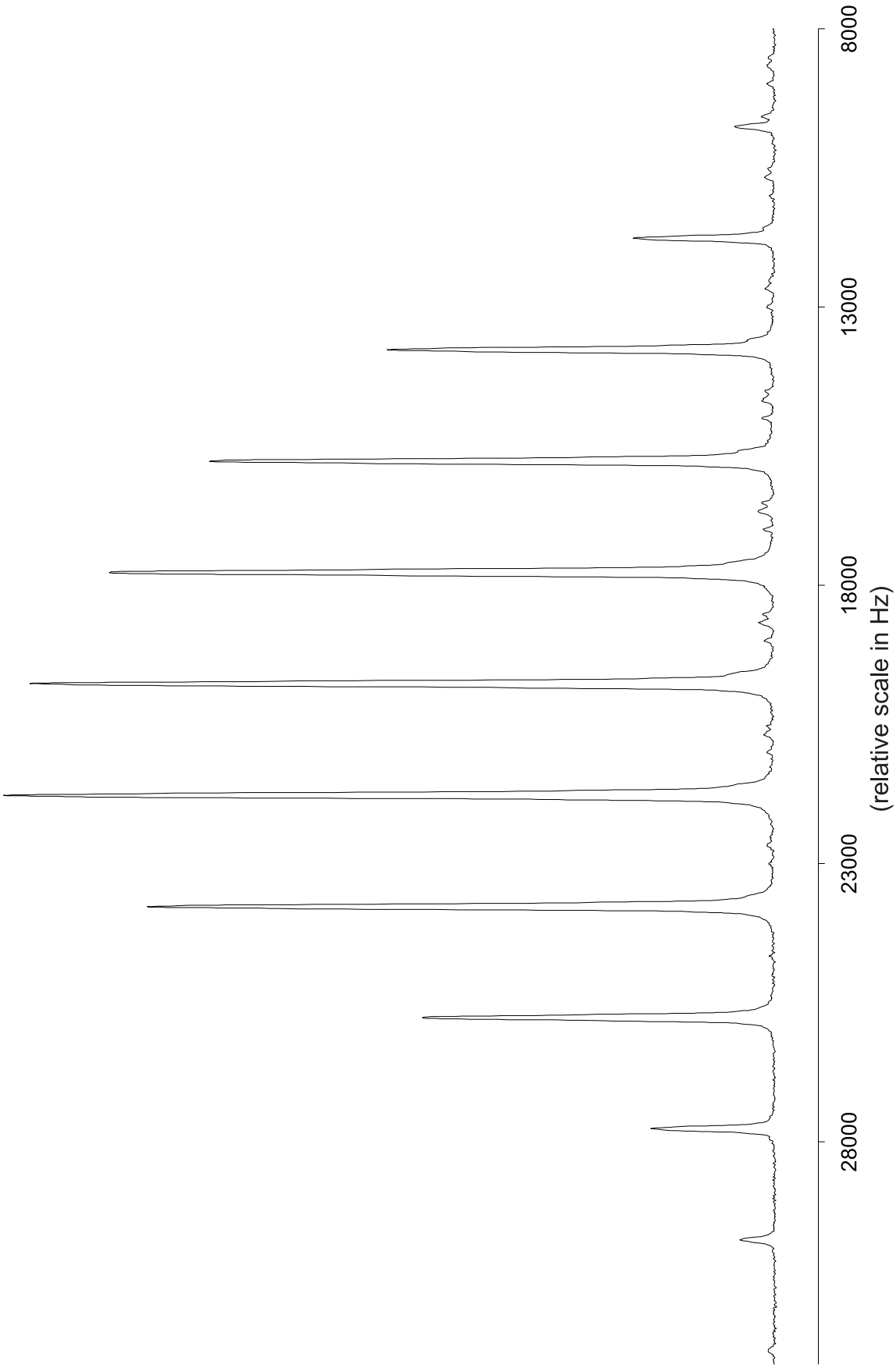

Figure E.19: CP/MAS ^{13}C-NMR spectrum (100.6 MHz) of ^{13}C-acetanilide at a spinning rate of 2000 Hz±2 Hz

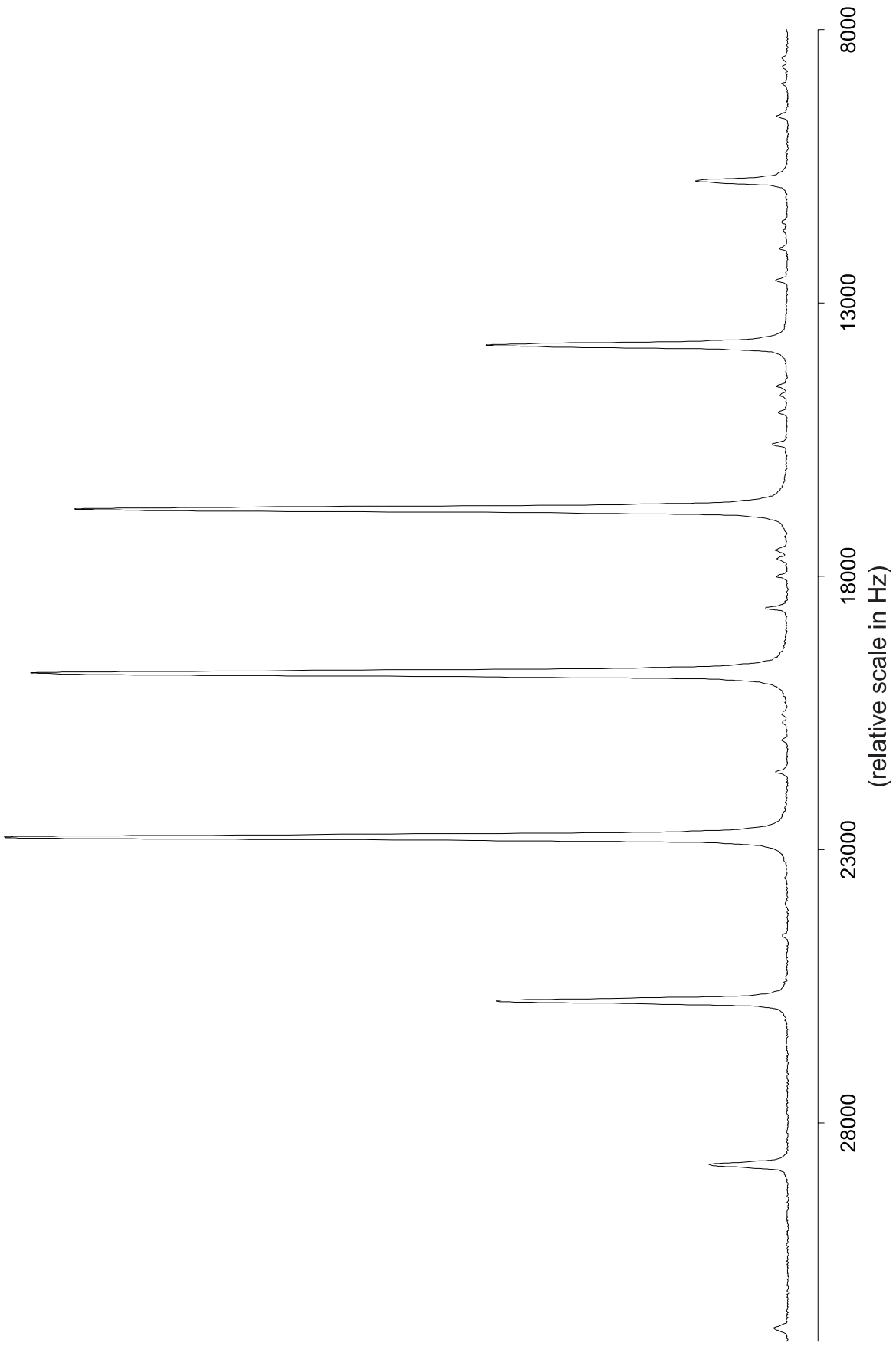

Figure E.20: CP/MAS ^{13}C-NMR spectrum (100.6 MHz) of ^{13}C-acetanilide at a spinning rate of 3000 Hz±2 Hz

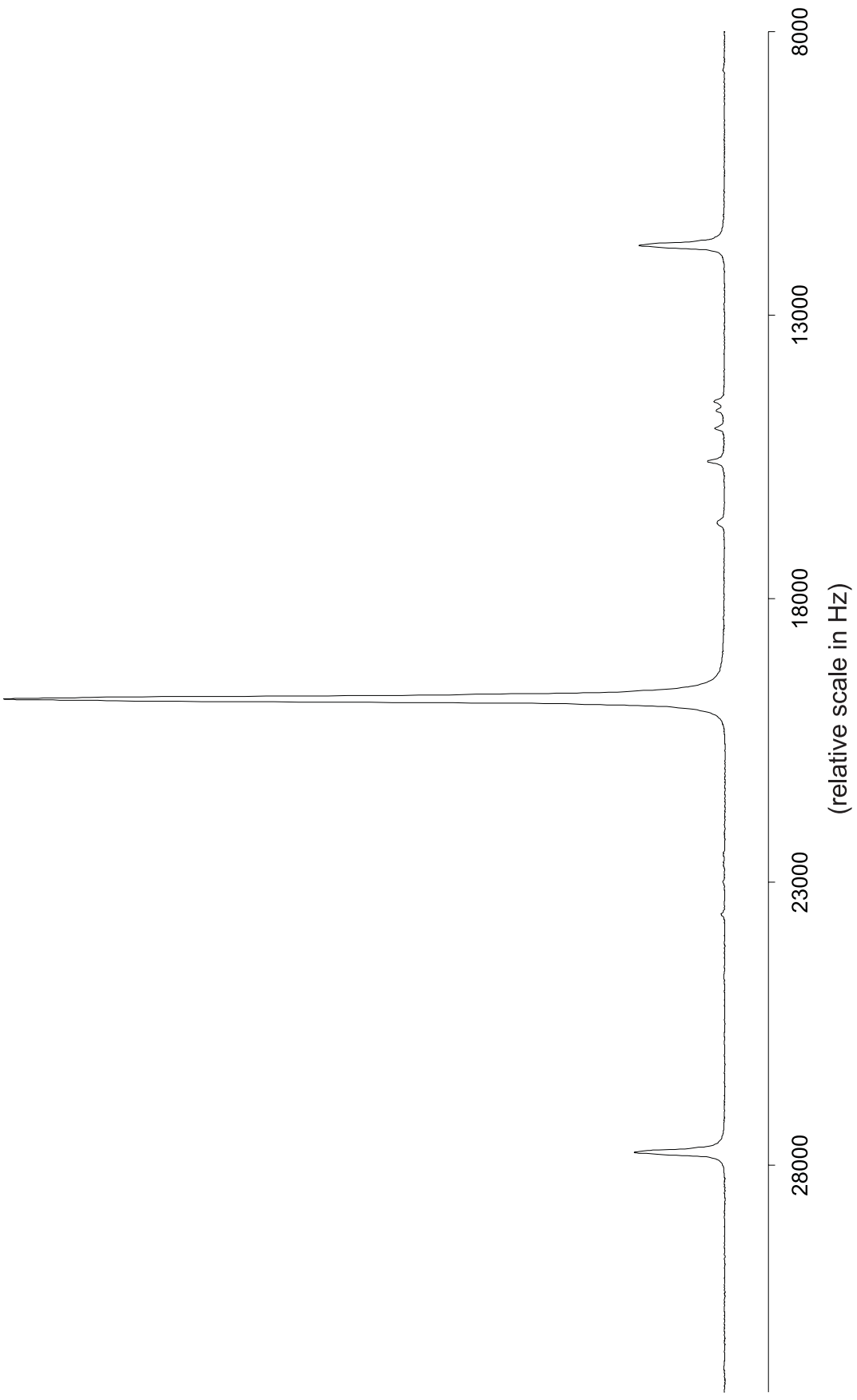

Figure E.21: CP/MAS ^{13}C-NMR spectrum (100.6 MHz) of ^{13}C-acetanilide at a spinning rate of 8000 Hz±2 Hz

Chapter F

Results

The X-Ray single crystal data of acetanilide the reported[1] orthorhombic structure. So we can expect to get comparable CP/MAS NMR spectra to Eichele *et al.* [23]. Eichele *et al.* simulated the central band of these spectra with a perturbation theory based simulation program. The input parameters for the simulation with *LanXSSQ* are listed in table (F.1). The relative tensor orientations and parameters were taken from the prementioned reference.

Figure (F.1) shows simulated central bands of acetanilide MAS spectra, at a spinning speed of 1991 Hz, in comparison to the experimental spectrum. Although the fast relaxation of the quadrupolar nucleus in these simulations is not considered (see page 36), the basic change in the spectrum with variation of the magnetic field is correct. The low field spectrum consists of the expected asymmetric doublet with comparable relative intensities and splitting of the two main signals. At higher field the resonance frequencies are almost combined to a single band. In Figure (F.2) the experimental and simulated spectrum at 4.7 T with two spinning sidebands is shown. The shape of the spinning sidebands is not modeled accurately, which is an additional indication, that the fast T_2 relaxation of the quadrupolar nucleus has to

[1] Acetanilide can crystalize in an orthorhomic or plate crystal system

be considered.

The lineshape of the simulated spectrum is different compared to the experiment caused by inhomogenities in the sample, which results in gaussian line-shapes. The simulated bands have the form of lorenzian functions, which are at the top narrower and at the bottom wider. It is possible to improve the band shapes, if gaussian broadening would be used.

The fast T_2 relaxation limit of the quadrupolar nucleus is implemented in *LanXSSQ* and simulations of ^{13}C-acetanilide MAS spectra at 8054 Hz and the experimental spectrum are shown in figure (F.3). The spectrum calculated with the changed version of *LanXSSQ* (including fast T_2 relaxation) is almost identical to simulations based on perturbation theory programs. Now, the spectrum consists of the expected two bands rather than three, but the relative intensities of the asymmetric doublet is not as good as simulations without considering the relaxation of the quadrupolar nucleus. Here it seems to be that the relaxation time of the quadrupole nucleus plays an important role in respect to the relative intensities of the asymmetric doublet.

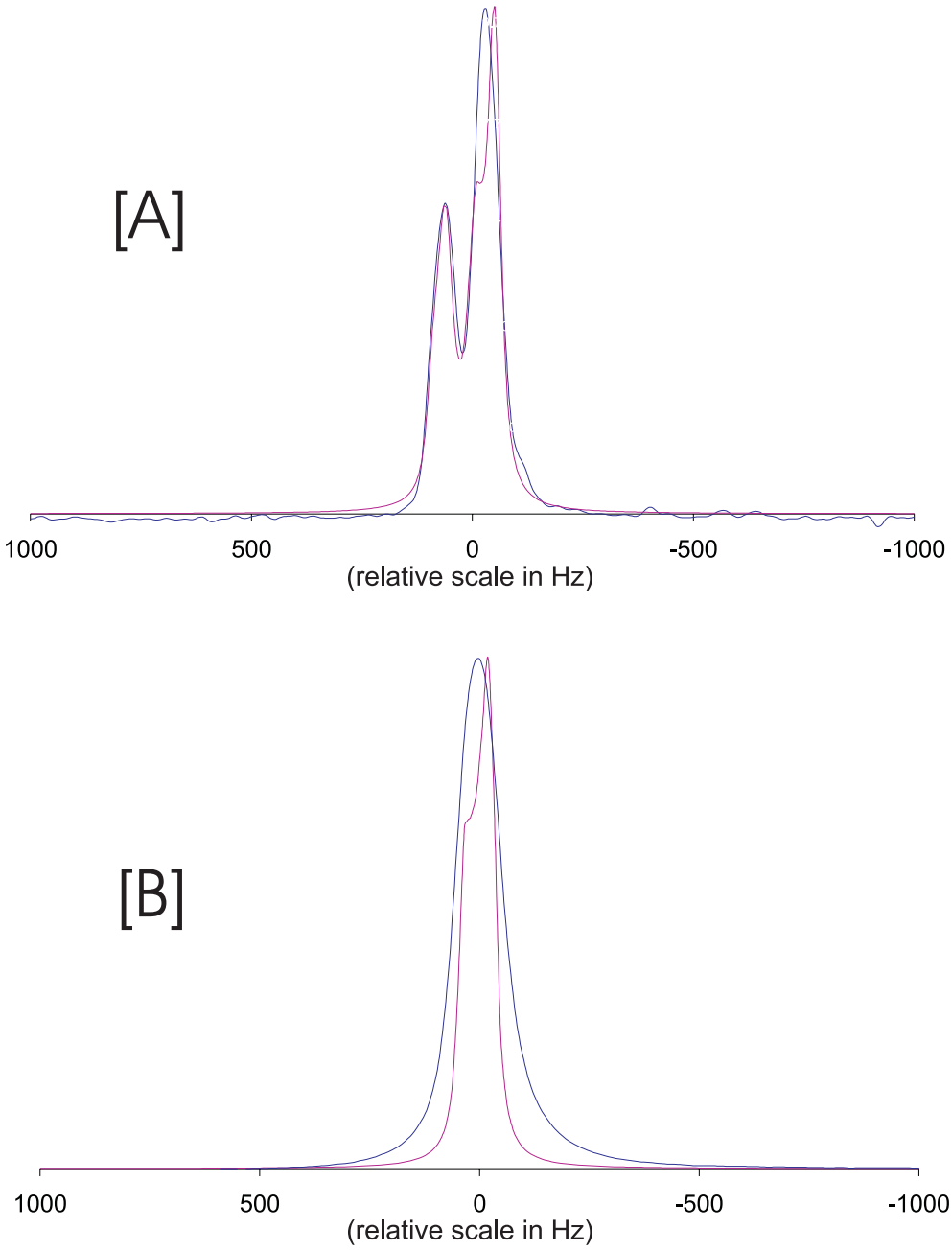

Figure F.1: Experimental and simulated central band of the MAS spectrum of the ^{13}C-^{14}N spin system in acetanilide. The experimental spectrum is represented through a blue and the simulated spectrum through the purple graph.

[A]: B_0=4.7 T, ν_R=1991 Hz

[B]: B_0=9.4 T, ν_R=8000 Hz

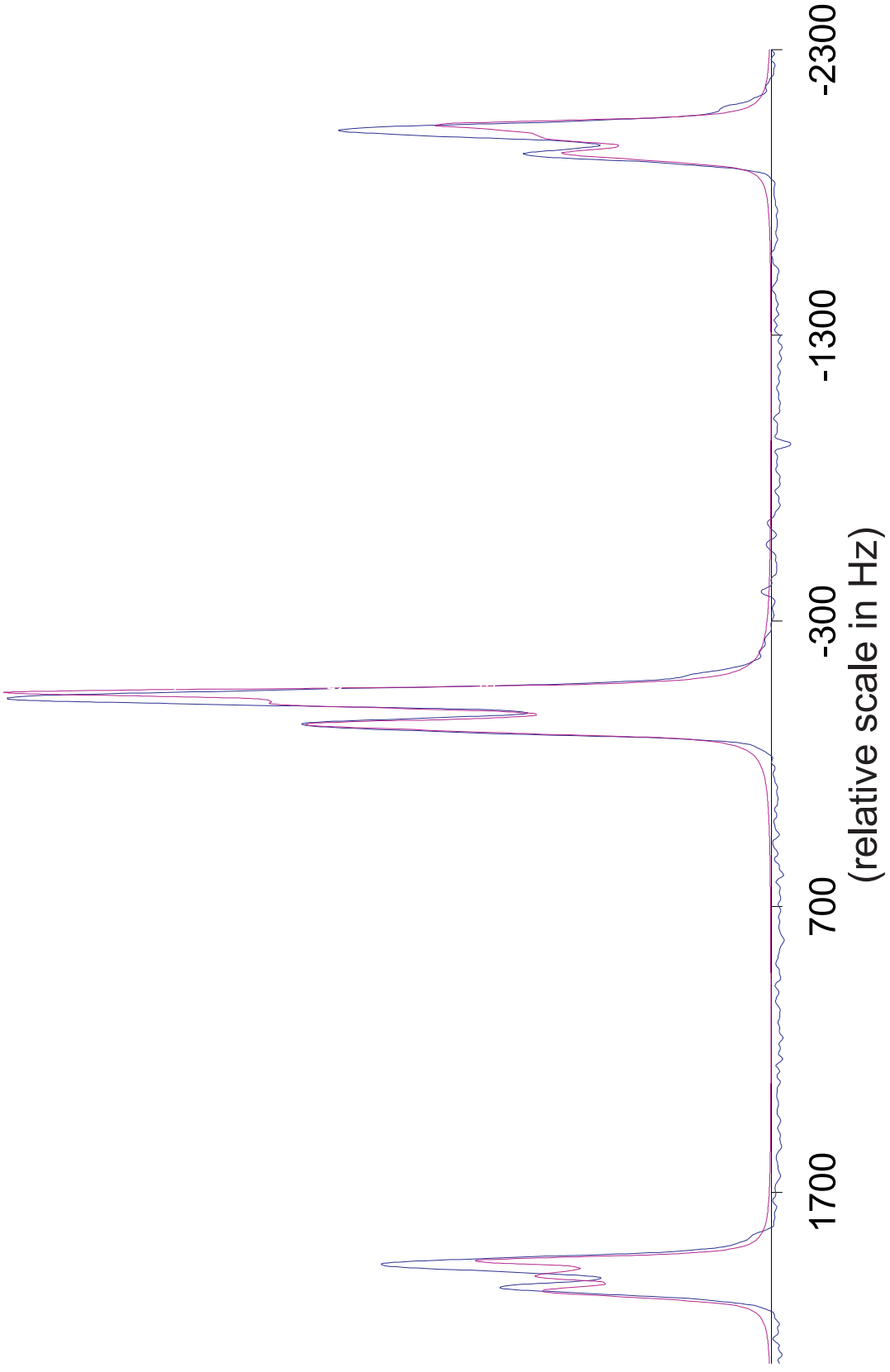

Figure F.2: Experimental and simulated MAS spectrum of the ^{13}C-^{14}N spin system in acetanilide with spinning side bands. The experimental spectrum is represented through a blue and the simulated spectrum through a purple line.

B_0=4.7 T, ν_R=1991 Hz

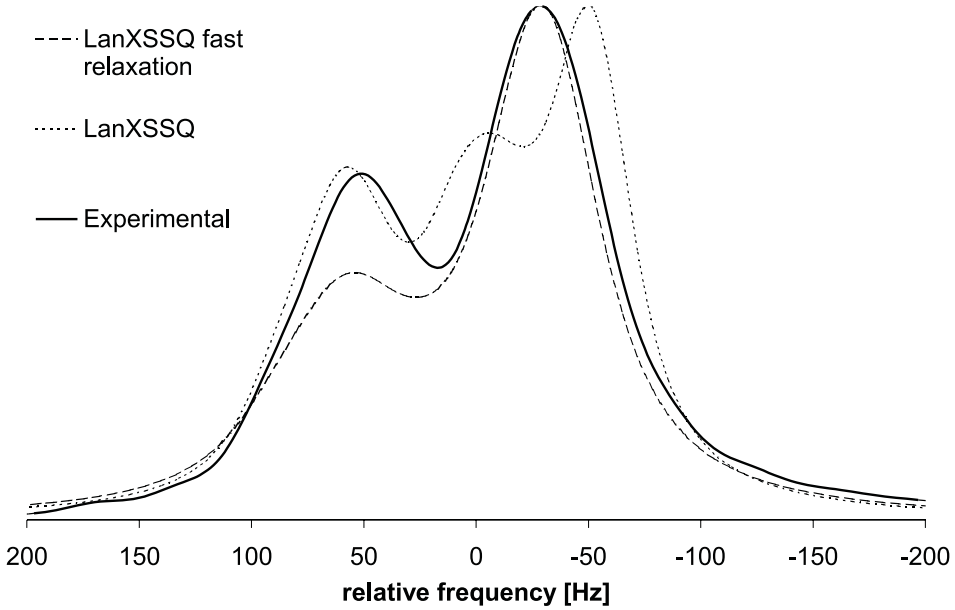

Figure F.3: Simulated spectra and experimental spectrum of the ^{13}C-^{14}N spin system in acetanilide with and without the T_2 relaxation of the quadrupolar nucleus.
Input parameters are listed in table (F.1), except the lorenzian broadening is set to 50 Hz.
B_0=4.7 T, ν_R=8054 Hz

Table F.1: Input parameters for the simulations of acetanilide MAS spectra

Spin system parameters

chemical shielding tensor		*quadrupole tensor*	
σ_{xx}	77 ppm	q_{xx}	0.624 MHz
σ_{yy}	4 ppm	q_{yy}	0.976 MHz
σ_{zz}	-81 ppm	q_{zz}	-1.6 MHz
α_σ	-30.0 °	α_q	-137.0 °
β_σ	0 °	β_q	0 °

atom coordinates

C: x and y	0.0 pm
C: z	134.8 pm
N: x, y and z	0.0 pm

Magnetic field dependent parameters

low magnetic field		*high magnetic field*	
B_0	4.7 T	B_0	9.4 T
ν_C	50.3 MHz	ν_C	100.6 MHz
ν_N	14.2 MHz	ν_N	28.4 MHz
ν_R	1991 Hz	ν_R	8000 Hz

Program specific parameters

γ increments	1024
molecule orientations	956
Floquet blocks	21
maximal Fourier components	11
Lorenzian broadening	25 Hz
cut off Hamiltonian elements	<0.2

Chapter G

Conclusions

This work presented a new, more general method for the simulation of MAS NMR spectra with quadrupolar interactions. The simulation program (*LanXSSQ*) was tested for the weak and strong quadrupole interaction limits. In case of weak quadrupole interaction, the spectra of acetanilide were considered and the program was compared with perturbation theory based calculations from Eichele *et al.* [23]. In case of approximately infinite quadrupole interaction the spin-$\frac{1}{2}$ coupled to a spin-$\frac{3}{2}$ system was considered and inverse perturbation theory based calculations [17] were compared with our simulation program. In both cases the original version of *LanXSSQ* didn't reproduce the perturbation theory based calculations, because our program didn't consider the fast T_2 relaxation of the quadrupolar nucleus. Relaxation terms could be included in the current formulation of *LanXSSQ*, which is not done at this stage. But the fast relaxation limit, which is equivalent to the assumption that the quadrupole nucleus is for all considered rotor phases in its eigenstate, was implemented in *LanXSSQ*. In this case our program reproduces the frequencies calculated with perturbation theory based programs, since this assumption is used in all today used simulation programs of this kind.

Most simulation programs consider only the central band of MAS NMR spectra.

The implementation of Floquet theory in *LanXSSQ* allows it also to simulate the spinning sidebands accurately. Simulation of spinning sidebands is especially useful because of the additional information content. Solid state spectra require large number of parameters. It is desirable to obtain as much experimental observation as possible to ensure good parameter assignments.

The formulation of average Hamiltonian theory to eliminate the fast quadrupolar spin dynamics time-scale is unique - especially in the context of a Floquet treatment. The theoretical formulation seems to work correctly, but it was shown, that quadrupolar spin relaxation has to be implemented in future versions of *LanXSSQ*. In most cases it would be enough to consider the fast relaxation limit of the quadrupolar nucleus, but it is worth implementing a more general formulation and see how different relaxation times affect the simulated spectrum - potentially giving a better fit to experimental spectra.

In acetanilide, for example, the perturbation approaches within the fast relaxation limit cannot reproduce the relative intensities of the asymmetric doublet. It is possible that in this case the fast relaxation approximation is not accurate enough.

After the implementation of the quadrupolar nucleus relaxation, spin systems with intermediate quadrupolar coupling can be considered - that is cases for which the quadrupolar interaction has the same magnitude as the Zeeman interaction. In such cases perturbation approaches are not valid. Examples of such spin system are ^{13}C coupled ^{35,37}Cl at low magnetic fields (e.g. 4.7 T) and ^{13}C coupled ^{59}Co in organo metallic complexes. *LanXSSQ* also handles multiple spin systems and chemical exchange.

Bibliography

[1] J. Herzfeld and A.E. Berger. *J. Chem. Phys.*, **73**:6021–6030, (1980).

[2] A.C. Olivieri, L. Frydman, and L.E. Diaz. *J. Magn. Reson.*, **75**:50–62, (1987).

[3] A.C. Olivieri. *J. Magn. Reson.*, **81**:201–205, (1989).

[4] R.K. Harris and A.C. Olivieri. *Progr. NMR Spectrosc.*, **24**:435–456, (1992).

[5] P. Grondona and A.C. Olivieri. *Conc. Magn. Reson.*, **5**:319–339, (1993).

[6] B.H. Suits, J. Šepa, and D. White. *J. Magn. Reson., Series A*, **120**:88–96, (1996).

[7] A.C. Olivieri, L. Frydman, M. Grasselli, and L.E. Diaz. *Magn. Reson. Chem.*, **26**:281–286, (1988).

[8] A.C. Olivieri, L. Frydman, M. Grasselli, and L.E. Diaz. *Magn. Reson. Chem.*, **26**:615–618, (1988).

[9] N.A. Davis, R.K. Harris, and A.C. Olivieri. *Molecular Physics*, **87**:669–677, (1996).

[10] S.H. Alarcón, A.C. Olivieri, S.A. Carss, and R.K. Harris. *Magn. Reson. Chem.*, **33**:603–606, (1995).

[11] R.K. Harris and R. Wasylishen. *J. Phys. Chem.*, **99**:10110–10113, (1995).

[12] S.H. Alarcón, A.C. Olivieri, S.A. Carss, and R.K. Harris. *Angew. Chem. Int. Ed. Engl.*, **33**:1624–1625, (1994).

[13] C. Filip, S. Hafner, I. Schnell, D.E. Demco, and H.W. Spiess. *Chem. Phys.*, **110**(1):423–440, (1998).

[14] C. A. McDowell and T. Nakai. *J. Chem. Phys.*, **96**:3452–3466, (1991).

[15] O. Weintraub and S. Vega. *J. Magn. Reson., Series A*, **105**:245–267, (1993).

[16] P. Hazendonk, A.D. Bain, P.H.M. Grondey, P.H.M. Harrison, and R.S. Dumont. Simulations of chemical exchange lineshapes in cpmas spectra using floquet theory and sparse matrix methods. (Submitted to the Journal of Magnetic Resonance).

[17] A.C. Olivieri. *J. Magn. Reson., Series A*, **101**:313–316, (1993).

[18] K. Eichele, R. Wasylishen, J. S. Grossert, and A.C. Olivieri. *J. Phys. Chem.*, **99**:10110–10113, (1995).

[19] E.M. Menger and W.S. Veeman. *J. Magn. Reson.*, **46**:257–268, (1982).

[20] A. S. Davydov. *Quantum Mechanics, Second Edition.* Pergamon International Library, (1993),388-392.

[21] M. Reed and B. Simon. *Methods of Modern Mathematical Physics,* **I** *Functional Analysis.* Academic Press, (1980),221-248.

[22] R.S. Dumont, P. Hazendonk, and A.D. Bain. Dual lanczos simulation of dynamic nmr spectra for systems with many spins or exchange sites. (Submitted to the Journal of Chemical Physics).

[23] K. Eichele, M.D. Lumsden, and R.E. Wasylishen. *J. Phys. Chem.*, **97**:8909–8916, (1993).

[24] S.W. Johnson, J. Eckert, M. Barthes, R.K. McMullan, and M. Muller. *J. Phys. Chem.*, **99**:16253–16260, (1995).

[25] H.J. Wasserman, R.R. Ryan, and S.P. Layne. *Acta Crystallogr.*, **C41**:783–785, (1984).